UNIVERSIDADE TECNOLÓGICA FEDERAL DO PARANÁ
PROGRAMA DE PÓS-GRADUAÇÃO EM ENGENHARIA ELÉTRICA E INFORMÁTICA INDUSTRIAL

MAYRON VINICIUS LOPES DE CAMARGO

DIGITAL TWIN IMPLEMENTATION AND PERFORMANCE EVALUATION IN THE LUBRICATION SYSTEM OF A HEAVY-DUTY DIESEL ENGINE

DISSERTAÇÃO

CURITIBA
2023

MAYRON VINICIUS LOPES DE CAMARGO

DIGITAL TWIN IMPLEMENTATION AND PERFORMANCE EVALUATION IN THE LUBRICATION SYSTEM OF A HEAVY-DUTY DIESEL ENGINE

Implementação e Avaliação de Desempenho da Aplicação de um Digital Twin no Sistema de Lubrificação de um Motor a Diesel de Serviço Pesado

Dissertação apresentado(a) como requisito para obtenção do título(grau) de Mestre em Engenharia Elétrica e Informática Industrial, da Universidade Tecnológica Federal do Paraná (UTFPR).

Orientador(a): Dr(a). Marco Aurelio Wehrmeister
Coorientador(a): Dr(a). Elder Oroski

CURITIBA

2023

Ministério da Educação
Universidade Tecnológica Federal do Paraná
Campus Curitiba

MAYRON VINICIUS LOPES DE CAMARGO

DIGITAL TWIN IMPLEMENTATION AND PERFORMANCE EVALUATION IN THE LUBRICATION SYSTEM OF A HEAVY-DUTY DIESEL ENGINE

Trabalho de pesquisa de mestrado apresentado como requisito para obtenção do título de Mestre Em Ciências da Universidade Tecnológica Federal do Paraná (UTFPR). Área de concentração: Engenharia De Computação.

Data de aprovação: 15 de Dezembro de 2023

Dr. Marco Aurelio Wehrmeister, Doutorado - Universidade Tecnológica Federal do Paraná

Dr. Elder Oroski, Doutorado - Universidade Tecnológica Federal do Paraná

Dr. Lucas Pioli Rehbein Kurten Ihlenfeld, Doutorado - Universidade Tecnológica Federal do Paraná

Dr. Ricardo Schumacher, Doutorado - Universidade Federal do Paraná (Ufpr)

Documento gerado pelo Sistema Acadêmico da UTFPR a partir dos dados da Ata de Defesa em 05/02/2024.

I dedicate this work to my family and friends,

for the moments of absence.

ACKNOWLEDGEMENTS

This work could not have been completed without the help of various individuals and/or institutions to whom I pay homage. Certainly, these paragraphs will not encompass all the people who were part of this important phase of my life. Therefore, I apologize in advance to those who are not mentioned in these words, but they can be assured that they are in my thoughts and gratitude.

To my family, for their affection, encouragement, and unwavering support in every moment of my life. To my advisor, who guided me on the paths to be followed and for the trust placed in me. To all the professors and colleagues in the department who directly and indirectly contributed to the completion of this work. In short, to all those who, in some way, contributed to the realization of this work.

First Law: A robot may not injure a human being or, through inaction, allow a human being to come to harm. Second Law: A robot must obey the orders given to it by human beings, except where such orders would conflict with the First Law. Third Law: A robot must protect its own existence as long as such protection does not conflict with the First and Second Laws (ASIMOV, Isaac, 1950).

RESUMO

CAMARGO, Mayron Vinicius Lopes de. **Implementação e Availiação de Performance de um *Digital Twin* em um Sistema de Lubrificação de um Motor Diesel de Aplicação Pesada**. 2023. 64 f. Dissertação (Mestrado em Engenharia Elétrica e Informática Industrial) – Universidade Tecnológica Federal do Paraná. Curitiba, 2023.

Este trabalho explora a aplicação da identificação de sistemas a um sistema de lubrificação encontrado em motores a diesel de aplicação pesada. Esses motores são equipados com uma bomba de óleo variável e um jato de pistão de refrigeração. O objetivo é estabelecer um modelo dinâmico que capture com precisão a relação entre o ciclo de trabalho das válvulas e os valores de pressão resultantes sob condições normais de operação na estrada, a serem usados como um *digital twin* do sistema. Além disso, o estudo visa determinar se um modelo recursivo simples pode descrever o sistema com precisão suficiente. Diferentes modelos lineares e não lineares foram avaliados e validados para identificar o melhor ajuste para o sistema. Em última análise, o sistema foi descrito usando um modelo Hammerstein-Wiener, resultando em um raiz quadrada do erro médio (NRMSE) de $86{,}58\%$ para a pressão na galeria principal e $89{,}76\%$ para a pressão na galeria do jato de refrigeração do pistão para os dados de validação.

Palavras-chave: Modelamento Caixa Preta. Modelamento de Sistemas Automotivos. Sensores e Atuadores Automotivos. Digital Twin. Identificação de Sistemas.

ABSTRACT

CAMARGO, Mayron Vinicius Lopes de. **Digital Twin Implementation and Performance Evaluation in the Lubrication System of a Heavy-Duty Diesel Engine**. 2023. 64 p. Dissertation (Bachelor's Degree in Electrical and Computer Engineering) – Universidade Tecnológica Federal do Paraná. Curitiba, 2023.

This work explores the application of system identification to a lubrication system found in heavy-duty diesel engines. These engines are equipped with a variable oil pump and a cooling piston jet. The objective is to establish a dynamic model that accurately captures the relationship between the duty cycle of the valves and the resulting pressure values under normal road operating conditions to be used as a digital twin of the system. Additionally, the study aims to determine whether a simple recursive model can sufficiently describe the system with enough precision. Different linear and nonlinear models were evaluated and validated to identify the best fit for the system. Ultimately, the system was described using a Hammerstein-Wiener model, resulting in an 86.58% Normalized Root Mean Squared Error (NRMSE) for main gallery pressure and 89.76% for piston cooling jet gallery pressure against the validation set.

Keywords: Black box modeling. Modeling of automotive systems. Automotive sensors and actuator. Digital Twin. System Identification.

LIST OF FIGURES

LIST OF TABLES

LIST OF ACRONYMS

INITIALISM	
ARMAX	Autoregressive Moving Average with Exogenous Inputs
ARX	Autoregressive with Exogenous Inputs
ECU	Electronic Control Unit
FPE	Final Prediction Error
HW	Hammerstein-Wiener
MAE	Mean Absolute Error
MAPE	Mean Absolute Percentage Error
MBE	Mean Bias Error
MIMO	Multiple-Input Multiple-Output
MISO	Multiple-Input Single-Output
MSE	Mean Square Error
NARX	Nonlinear Autoregressive with Exogenous Inputs
NRMSE	Normalized Root Mean Square Error
OCV	Oil Control Valve
PCJ	Piston Cooling Jet
PWL	Piecewise Linear
RAE	Relative Absolute Error
RRMSE	Relative Root Mean Squared Error
RSE	Relative Squared Error
XCP	Extended Calibration Protocol

LIST OF SYMBOLS

NOTATIONS

$\nu(k)$	Noise vector	
$A(q)$	Polynomial function of the lag operator q^{-n} for the outputs	
$B(q)$	Polynomial function of the lag operator q^{-1} for the inputs	
$C(q)$	Polynomial function of the lag operator q for the error	
q^{-1}	Lag operator	
r_{uy}	Correlation between $u(k)$ and $y(k)$	
T_s	Sampling period	[s]

CONTENTS

1 INTRODUCTION

This work explores the practical application of a digital twin using system identification techniques to identify a lubrication system found in heavy-duty diesel engines. The digital twin described here is the dynamical description of the system's dynamic behavior using simple equations in function of indirect measurements.

1.1 TOPIC DELIMITATION

This dissertation is dedicated to the exploration of system identification models as they are applied to the lubrication system within a heavy-duty diesel engine. The primary focus of this study is the practical application of system identification techniques to real-world data, with the aim of developing a model that accurately characterizes the dynamic behavior of this specific system. The scope of this research is confined exclusively to the lubrication system component of the engine and is specifically centered around the utilization of regressive models for modeling purposes.The use of machine learning techniques such artificial neural networks were not considered in this works, since the main idea is the use of recursive models that can be easily implemented in micro controllers running in real time.

1.2 PROBLEMS AND ASSUMPTIONS

Extensive literature exists on the study and identification of diesel engine emission-related components. One such study uses artificial neural networks to estimate the fuel injected by the engine(ZHANG, 2022). Different data-driven control techniques and future challenges related to engine after-treatment can be found in literature(JIANG *et al.*, 2022). Studies show the use of different model structures to predict NOx[1] emissions, comparing accuracy in steady-state and transient conditions(SMITS *et al.*, 2022). Also, the use of system identification to study exhaust gas control systems for diesel particulate filter regeneration aims to achieve efficient regeneration(HUANG *et al.*, 2023).

There are few studies that focus on modeling oil systems in diesel engines. Hence, this work explores system identification techniques using both linear and nonlinear models to propose

[1] Oxides of nitrogen are pollutant gases released during combustion(THOMAS, 1997).

a digital twin representation for the system in study. A digital twin refers to a virtual representation of a physical entity or system, such as a product, process, or environment, which is created through the integration of real-time data from the physical counterpart and digital simulations (NIKOLAKIS *et al.*, 2019). This technology allows for monitoring, analysis, and optimization of the physical system's performance, enabling a deeper understanding of its behavior, predicting potential issues, and facilitating data-driven decision-making for improvements(WANG *et al.*, 2021).

This research centers on the challenge of characterizing the dynamic behavior of a complex system using a simplified regression model, with a primary focus on modeling the system itself. Assumptions are made that the collected variables encompass the core aspects of the system, and their interrelationships can be adequately represented, even through linear models. These assumptions are grounded in extensive knowledge and prior studies of lubrication systems, where key variables influencing system behavior have been identified. Nonetheless, the possibility is acknowledged that linear dynamical systems may not fully capture the intricacies of the system's dynamics, potentially necessitating more advanced modeling techniques.

1.3 OBJECTIVES

1.3.1 Main Objective

The objective of this study is to apply system identification techniques to obtain a mathematical model capable of describing the dynamics of a real lubrication system applied in diesel engines, which can be used as a digital twin of the actual system.

1.3.2 Specific Objectives

The specific objectives are as follows:

1. To investigate various types of mathematical models and gain a comprehensive understanding of their behavior in relation to the behavior of the system;
2. Identify and analyze existing mathematical models commonly used;
3. Apply the selected mathematical models to the collected data and assess their performance in accurately predicting engine oil pressure behavior;

4. Evaluate the performance and accuracy of the mathematical models by comparing their predictions with the collected data from the diesel engine, enabling a quantitative assessment of their reliability and effectiveness;

5. Improve the overall understanding of the system under investigation through a comprehensive analysis and interpretation of the model results, identifying any discrepancies or areas where further refinement is required to enhance the accuracy and reliability of the mathematical model;

6. Develop a digital twin implementation of the lubrication system that is capable of describing the system's dynamic behavior.

1.4 JUSTIFICATION

The lubrication system is essential within an engine, serving as a key for enhancing its reliability and durability. This intricate system ensures the smooth operation of the engine's moving components. A delicate, continuous film of oil is meticulously pumped to envelop and glide between these components, fulfilling two primary objectives. Firstly, it serves as a guardian of the engine's well-being by meticulously lubricating bearing surfaces to mitigate wear and friction. Secondly, it acts as a vigilant sentinel, dissipating the heat generated from friction to maintain the optimal operational temperature of the bearings. Such a vital role demands precision and control, a responsibility borne by the Electronic Control Unit (ECU).

The importance of the engine's lubrication system cannot be overstated. Despite its behind-the-scenes operation, its fragility underscores its critical role. A malfunction or damage to this system can lead to catastrophic consequences in a remarkably short span. This vulnerability arises from the immense energy generated by friction within the engine's mechanical components. Therefore, an in-depth understanding of this system isn't merely advantageous; it is integral to the very existence of the engine itself (Engineers Edge, 2023).

Within this intricate system, a group of control components assumes a pivotal role. These components are responsible for managing the flow of oil within the engine and regulating oil pressure in the galleries. In the following section, one will embark on an extensive exploration of these crucial elements, unveiling their complexities and functions in finer detail.

The significance of developing a precise model for the oil system extends beyond the realm of theoretical understanding. It holds practical implications for the industry, offering the

potential for predictive maintenance and performance enhancement throughout the engine's life cycle. A robust model that accurately describes and predicts oil pressure behavior aids in the early identification of potential issues. Additionally, it can communicate vital points of concern to the vehicle's ECU, enabling analysis and improvements to the overall system performance.

By incorporating the concept of a "digital twin," which refers to a virtual counterpart of a physical entity created through the integration of real-time data and digital simulations (NIKOLAKIS *et al.*, 2019), it will be developed a mathematical model. This model will serve as a dynamic representation of our real-world system, facilitating our endeavor to understand and analyze its behavior. The model is a simple description of the dynamic behavior in real time using indirect measurements.

This implementation holds potential significance for the industry, as it can provide assistance in various aspects. An illustrative application involves its use for monitoring the operational status of a system. When the measurements of the system align with the model, it indicates smooth functioning. Conversely, deviations between the system and the model can serve as signals, aiding in the diagnosis of potential issues with the system.

1.5 METHODOLOGICAL PROCEDURES

This study begins with the data collection from a heavy-duty diesel vehicle operating under real-world conditions. Key variables, crucial for our analysis, were gathered using a designated automotive protocol called Extended Calibration Protocol (XCP). This dataset served as the primary input for subsequent modeling activities, the details of which will be expounded upon in the following sections.

The collected data was then processed and utilized to feed various model topologies, which will be elaborated upon later in this document. These models were fine-tuned and optimized to best align with the acquired dataset, thereby ensuring their accuracy and effectiveness in capturing the system's dynamic behavior.

To assess and compare the performance of these models, rigorous analysis and evaluation procedures were employed. The results obtained from each model were scrutinized, and the most promising outcomes, demonstrating superior alignment with the collected data, were singled out and highlighted for further discussion.

This methodological procedure provides a comprehensive overview of the data collection, modeling, and evaluation processes that form the foundation of our study. Subsequent

sections will delve into the specific details of these methodologies.

1.6 DOCUMENT STRUCTURE

This dissertation is organized into five distinct sections, each contributing to a comprehensive exploration of the study's topic:

In Chapter 2 one will delve into a thorough review of the relevant literature. This is essential for establishing a foundation of knowledge related to the subject matter. It presents an overview of key concepts, theories, and prior research, helping readers understand the evolution and background of the study.

Chapter 3 details the research methodology employed in this study. It outlines the research design, data collection methods, and mathematical simplifications. The section provides a clear explanation of how the study was conducted, ensuring transparency and replicability.

Chapter 4 presents and discusses the findings of the study. The results are analyzed and interpreted in the context of the research questions or hypotheses. Visual aids such as tables, charts, and graphs were included to enhance the presentation of results.

Finally, chapter 5 encapsulates the study's conclusions and implications. It summarizes the key findings, discusses their significance, and relates them to the research objectives. Additionally, this section may suggest areas for further research and reflect on the broader implications of the study's outcomes.

2 LITERATURE REVIEW

In this chapter, one can find two main sections. The first section will thoroughly examine the concepts relevant to the system under study. The second section will delve into the theory of system identification, giving the notion of its principles and applications.

2.1 HEAVY DUTY DIESEL ENGINE

A diesel engine, a type of compression-ignition engine, utilizes diesel as its primary fuel source (AGARWAL *et al.*, 2008). Typically, in on-road applications and trucks, a four-stroke diesel engine is employed (NAIK *et al.*, 2015). Diesel engines employ various fuel injection methods, with direct injection being highly used in contemporary applications. Diesel engines find extensive use in heavy-duty scenarios, encompassing trucks, buses, specific off-road vehicles, marine engines, generators, and more(HOANG, 2020). They are often categorized as low-speed, medium-speed, or high-speed engines, with high-speed engines capable of operating at speeds exceeding 1000 RPM (XIN, 2011).

Diesel engine boasts the highest thermal efficiency compared to all other internal and external combustion engines, primarily owing to its high expansion ratio (LEONE *et al.*, 2015). In a diesel engine, the combustion chamber initially receives only air before undergoing compression. This air is subsequently compressed within a range of ratios, typically between 15:1 and 23:1. The elevated compression ratio results in a significant rise in temperature within the combustion chamber (KLEIN, 1991). The injection process is constructed to disperse diesel fuel in minute droplets. These diesel droplets, upon contact with the intensely heated and compressed air, spontaneously ignite, initiating the combustion process(AGRAWAL, 2022). During the initial phase of the power stroke, the combustion unfolds at a nearly constant pressure (REIF, 2010).

The lubrication system plays a pivotal role in a diesel engine, serving multiple essential functions such as (i) friction reduction; (ii) temperature control; and (iii) mechanical component cleaning (NEEDELMAN; MADHAVAN, 1988). In order to illustrate the flow of oil within an engine, one can simplify the process into several distinct steps, as depicted in Figure 1:

1. The oil pump draws oil from the oil pan (Figure 1, component 1), where it is stored;

2. The pump (Figure 1, component 2) then directs the oil to the primary bearings of the

crankshaft (Figure 1, component 3), where linear energy is converted into rotational energy;

3. Subsequently, the oil traverses through small oil passages drilled within the crankshaft, ultimately reaching the rod bearings (Figure 1, component 4);
4. From there, it continues its path via an oil conduit to the cylinder head (Figure 1, component 5);
5. Within the engine, the oil circulates through designated oil galleries (Figure 1, component 6), nourishing the camshaft (Figure 1, component 7) bearings and valves;
6. Finally, the oil is dispersed to the pistons, piston rings, and wrist pins, which receive oil thrown off from the connecting rod bearings;

Figure 1 – Diesel engine simplified lubrication components and structure.

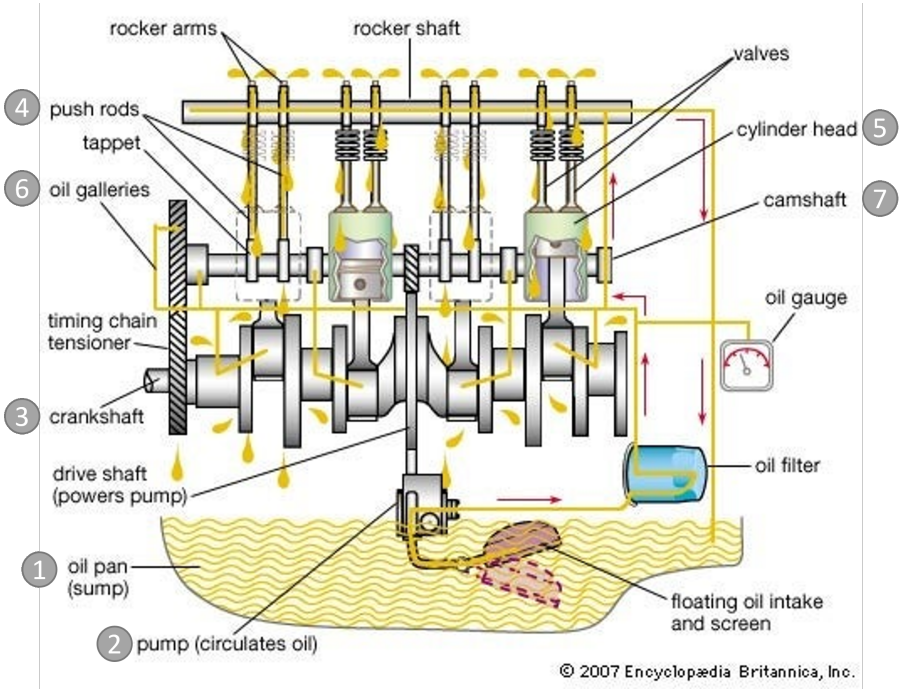

Source: Lubricants (2023).

2.2 OIL SYSTEM

Lubrication systems play a crucial role in managing engine thermal behavior (MARATHE *et al.*, 2022). The first technique explores the implementation of a variable oil pump, while the second technique examines the utilization of piston cooling to regulate the oil flow demanded by the engine.

2.2.1 Variable Oil Pump

The utilization of variable oil pumps is commonly employed in diesel engines to regulate the overall oil flow to the engine (ZHANG *et al.*, 2019). Different configurations of variable oil pumps have demonstrated a potential reduction of up to 3.4% in fuel consumption in modern diesel engines (BRACE *et al.*, 2009). Typically, the oil pump is connected to the engine crankshaft, resulting in oil flow variations corresponding to changes in engine speed (ZHANG *et al.*, 2019).

An engine that has a variable oil pump system has its control of the oil pressure in the main gallery achieved through a variable oil pump, controlled by an external electrical control valve called OCV. This valve regulates the re-circulation of oil to the pump, subsequently influencing the position of the rotor. When the valve opens, the flow is directed into the chamber, exerting pressure on the spring that holds the rotor in its main position (WANG *et al.*, 2012). Typically, the spring is positioned to enable maximum flow. However, when the valve is adjusted, compressing the spring, the rotor's position changes, resulting in a reduction in the volume between each rotor blade flap (LOGANATHAN *et al.*, 2011). Consequently, a smaller gap between the flaps leads to a decrease in the oil flow produced by the pump, subsequently reducing the system's pressure(WANG *et al.*, 2012). This technique effectively reduces flow when there is no demand from the consumers, resulting in lower energy consumption by the pump (LIU; ZHAI, 2023). Figure 2 illustrates the structure of a variable oil pump with its rotor in the center and the sprint that changes the rotor flaps position at the right-hand side of the rotor.

The oil pump is directly connected to the crankshaft, which means that its rotational velocity is directly proportional to the crankshaft speed (ZHANG *et al.*, 2019). Consequently, the flow rate of the pump is also directly influenced by the engine speed. However, the pressure variation within the system is subject to changes based on the system's constraints. These constraints are typically associated with the oil system consumers, which can vary during engine operation (LIU; ZHAI, 2023).

2.2.2 Piston Cooling Jet

In this study, another technique implemented in the engine is the utilization of a PCJ. By directing an oil jet to an internal gallery within the piston, a cooling piston oil system can enhance heat transfer and reduce piston temperature, particularly in low-speed diesel engines (BUSH;

Figure 2 – Structure of a variable oil pump.

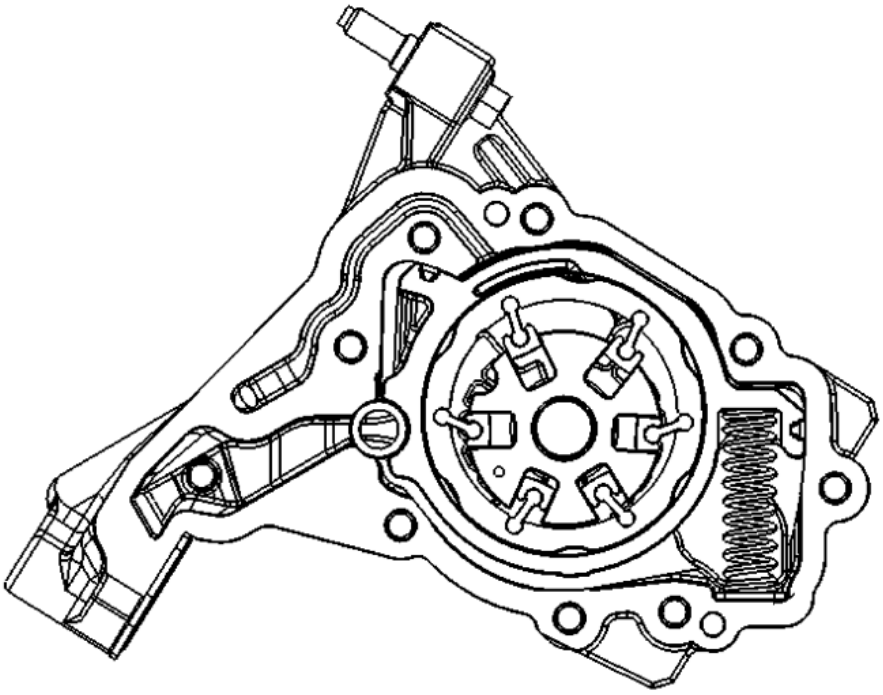

Source: Zhang *et al.* (2019).

LONDON, 1966). Depending on the operating conditions, this technique has demonstrated the potential to lower piston temperature by up to 80°C (LUFF *et al.*, 2012). In the 1990s, this technique was adapted for turbocharged[1] diesel engines operating at higher engine speeds by increasing the oil flow rates, resulting in a notable decrease in piston temperature (LEITES; CAMARGO, 1993). Currently, this system is commonly employed in modern heavy-duty turbo diesel engines.

The system comprises a piston-cooling jet nozzle, which is connected to an oil gallery and positioned inside the engine, pointing towards the engine piston's back. Various nozzle structures can be observed in Figure 3. The flow of the nozzle is regulated by a valve that controls the oil flow to the oil gallery, where the nozzle is connected. By manipulating the flow through this valve, the flow rate of the nozzle can be effectively controlled.

The design in Figure 3 (a) and (b) is used at a specific oil pressure (typically 2 to 2.5 bar) generated by the oil pump during the engine running, the spring-loaded ball valve, which is housed inside the ball valve housing, opens, and oil squirts at a precisely defined angle onto the underside of the piston crown. The purpose of the ball valve is to ensure that there is no cooling oil squirting at the piston underside when the engine is running at low load or idle condition and

[1] Engines mounted with a turbocharger that can operate with intake pressures higher than ambient pressure (LUMSDEN *et al.*, 2009).

Figure 3 – Different nozzles types for a piston cooling jet. (a) and (b) show jet nozzles with ball valve housing at the inlet. (c), no ball valve housing is provided at the inlet of the jet nozzle.

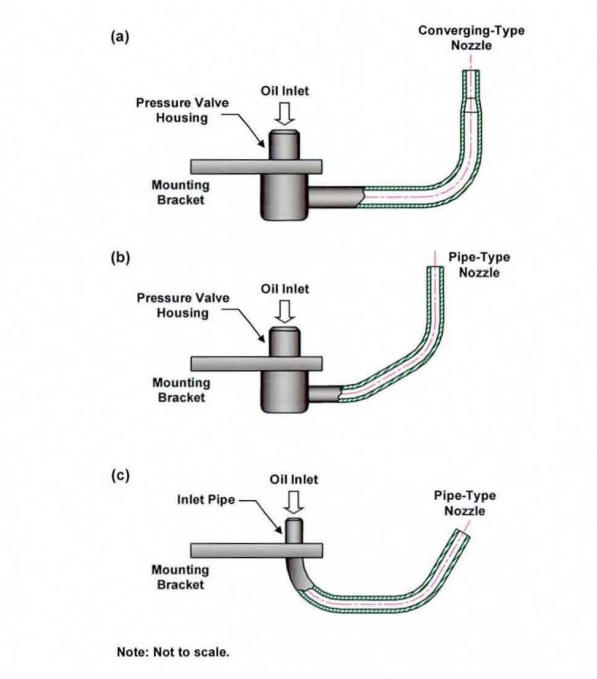

Source: Ting (2007).

that the piston temperature is still maintained dose to its ideal thermal operating levels. However, when an engine is running at a high load, high-pressure cooling oil driven by the oil pump will pass through the jet nozzle by pressing the ball valve, and the cooling oil flows through the orifice. The design shown in Figure 3 (c) ensures that the jet nozzle keeps squirting cooling oil to the piston underside surface whenever the engine is running. Therefore, this type of jet nozzle is used for heavily thermally loaded engines that require piston cooling at all load conditions(TING, 2007).

2.3 SYSTEMS IDENTIFICATION

This section will focus on the exploration of different types of models that are studied in this work. Each subsection will provide a brief introduction to the model and its corresponding mathematical equation. The models will be divided into linear and nonlinear, and each category will be explored independently. First, it will present some concepts involving system identification and later in this section, it will explore the models and metrics commonly used.

2.3.1 System Identification Steps

Finding a model structure that accurately represents a physical system with sufficient precision poses a significant challenge. The process of finding a model solution solely based on mathematical and physical concepts is known as white box modeling (AGUIRRE, 2004). In contrast, *black box* modeling does not require any prior knowledge about the system (AGUIRRE, 2004). Black box modeling involves analyzing and using data to develop a mathematical model (LJUNG, 1998).

Regarding the system identification process using black box modeling, Aguirre *et al.* (1998) outline several steps: (i) data acquisition; (ii) mathematical representation; (iii) model structure; (iv) parameter estimation; and (v) model validation.

2.3.1.1 Data Acquisition

The objective of the data acquisition process is to gather data that can accurately represent the real system. This initial step is crucial as it determines whether the identified model will be representative (AGUIRRE, 2004). Poor data collection can lead to a poorly represented system.

When choosing input signals, $u(k)$, it is important to assess their correlation with the output signal, $y(k)$. This can be achieved using the cross-correlation function, as shown in Equation 1.

$$r_{uy}(n) = \frac{1}{N} \sum_{k=1}^{N-n} u(k)y(k+n), \tag{1}$$

here, $r_{uy} \in \mathbb{R}$ represents the correlation between the signals, $n \in \mathbb{N}$ is a relative sample delay, $u(k) \in \mathbb{R}$ is the input signal, $y(k) \in \mathbb{R}$ is the output signal, and $N \in \mathbb{N}$ is the number of samples.

If $r_{uy}(n) > 0$, it indicates a positive correlation, meaning the signals have the same direction. If one signal increases, the other will also increase. Conversely, if $r_{uy}(n) < 0$, the signals have a negative correlation or opposite directions, where an increase in one signal corresponds to a decrease in the other. If $r_{uy}(n) \approx 0$, the signals have no correlation, and such an input signal can be discarded for consideration in the mathematical model.

Furthermore, the selected signals must provide a comprehensive representation of the system. This implies that the signals should contain a wide range of frequency components to effectively excite all the components of the real system (AGUIRRE, 2004). The frequency com-

ponent band that covers the entire range of interest is referred to as a "white signal" (AGUIRRE, 2004). If the collected signal does not contain all these frequency components, the identification process may fail to accurately model the dynamic behavior of the output signal that was not adequately excited by the input signal.

It is important to notice that the data collection for the signals must be made in a way that a wide range of combinations can be checked. This way it is possible to guarantee that the dynamic behavior of the system is being excited in all frequency components. When it is not possible to excite the system in such a way, the best option is to restrict the data around the operation point of the system and vary the conditions as much as possible. This way it is possible to ensure that the model can describe the dynamical behavior with enough precision around the operation point and sometimes can be linearized around it.

2.3.2 Sampling Time

The term sampling period, T_s, corresponds to the time between one collected sample and the next. When the data collection process selects only certain points of time, the data becomes discrete, and therefore the signal becomes discrete. To determine a value for T_s, the main reference in this matter is the Nyquist criterion, which states that the sampling frequency should be at least twice the maximum frequency component of the signal of interest.

However, Aguirre (2004) suggest a value for T_s between 5 and 10 times the maximum frequency component of the signal. For black box identification, Aguirre (2004) also proposes that the value of T_s should be as small as possible. Nevertheless, if the samples become redundant, meaning $u(k) \approx u(k+1)$, this signal can be sub-sampled. The sub-sampling process is also known as decimation. For an oversampled signal, the cross-correlation function, Equation 1, has low decaying values. Aguirre (2004) also suggests using decimation until the cross-correlation function reaches its valley within a range of 5 to 25 delays. Considering that in this case, the data acquisition process discretizes the continuous signal, the mathematical representation of the model should represent a discretized system.

2.3.3 Types of Models

2.3.3.1 ARX

The Autoregressive with Exogenous Inputs model, also known as ARX, is a mathematical framework that describes a system in which the output variable is modeled as a linear combination of its past values and external input variables (LJUNG *et al.*, 1987). It is defined in (2) in function of q^{-1} which is the lag operator where -1 means one sample lag.

$$A(q)\,y(k) = B(q)\,u(k) + \nu(k), \tag{2}$$

in which $A(q) \in \mathbb{R}^{N_y}$ is the polynomial function of the lag operator for the outputs, $y(k) \in \mathbb{R}^{N_y}$ represents the discrete-time system's outputs, $B(q) \in \mathbb{R}^{N_u}$ is the polynomial function of the lag operator q for the inputs, $u(k) \in \mathbb{R}^{N_u}$ is a vector representing the discrete-time inputs of the system, $N_u \in \mathbb{Z}$ the number of input signals, $N_y \in \mathbb{Z}$ the number of output signals, and $\nu(k) \in \mathbb{R}^{N_y}$ is the noise component for each output. In this type of modeling, the noise $\nu(k)$ is considered white noise. As this is a simple linear regressive model, linear optimization algorithms can be used to estimate its parameters. The operator $A(q)$ and $B(q)$ can be defined as follows:

$$A(q) = 1 - a_1 q^{-1} - ... - a_n q^{-n_a}, \tag{3}$$

$$B(q) = b_1 q^{-1} + ... + b_n q^{-n_b}, \tag{4}$$

where $a_1, \cdots, a_n, b_1, \cdots, b_n \in \mathbb{Z}$ represent the coefficients of the system, q^{-1} is the lag operator, representing one sample delay, and n_a,$n_b \in \mathbb{R}$ define the operators' regressor order.

2.3.3.2 ARMAX

An Autoregressive Moving Average with Exogenous Inputs model, also known as ARMAX model, is a variation of the ARX model in which a moving average component is added to the equation for ARX shown in (2) (LJUNG *et al.*, 1987). The resulting equation can be described as:

$$A(q)\,y(k) = B(q)\,u(k) + C(q)\,\nu(k), \tag{5}$$

in which $C(q) \in \mathbb{R}^{N_y}$ is a polynomial delay operator for the noise $\nu(k) \in \mathbb{R}^{N_y}$. Different from an ARX, for an ARMAX model $C(q)$ can be defined as:

$$C(q) = 1 + c_1 q^{-1} + \cdots + c_n q^{-n_c}, \tag{6}$$

here $c_1, \cdots, c_n \in \mathbb{R}$ represents the coefficient of the moving average component for the noise.

2.3.3.3 Hammerstein-Wiener

The Hammerstein model can be defined as a series connection of a dynamic model with a static nonlinear function (MÜNCHHOF; ISERMANN, 2011). As an example, consider the discrete dynamical system, with $k \in \mathbb{Z}$, with input $w(k) \in \mathbb{R}$, and $v(k) \in \mathbb{R}$ defined by:

$$H(z) = \frac{V(z)}{W(z)} = \frac{\mathcal{Z}\{v(k)\}}{\mathcal{Z}\{w(k)\}}, \tag{7}$$

in which $\mathcal{Z}\{.\}$ is the Z transform operator.

The static nonlinearity can be defined as any nonlinear function $f(\cdot) : \mathbb{R}^{\alpha} \rightarrow \mathbb{R}^{\beta}$, being α and $\beta \in \mathbb{N}$. In a dynamic block, the current output depends on its past values, while the output of static blocks depends only on its current inputs (LJUNG *et al.*, 1987). When the static nonlinear function $f(\cdot)$ is connected to the input signal $w(k)$ of the dynamical system $H(z)$, the representation is called Hammerstein model. Hence, the output $y(k)$ of the Hammerstein model is equal to the output $v(k)$ of the dynamical system. The connections between the functions can be seen in Figure 4.

Figure 4 – Representation of a Hammerstein model where the input signal $u(k)$ is connected to the static nonlinear function $f(\cdot)$ and the output of the dynamic model $v(k)$ is the final output of Hammerstein model $y(k)$.

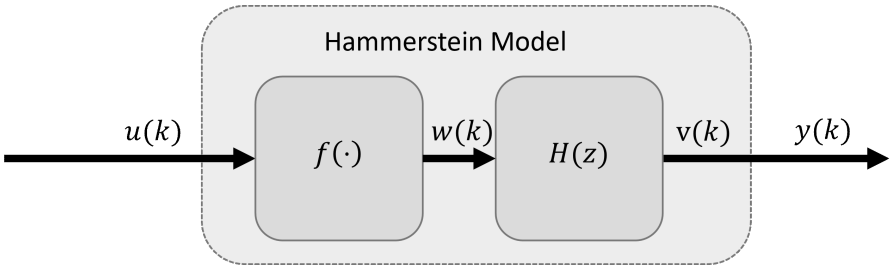

Source: Author.

However, when this same type of nonlinear function $f(\cdot)$ is connected to the output of the linear model $v(k)$ it results in a Wiener model. In this configuration, the input of the Wiener model $u(k)$ is the same as the input $w(k)$ of the dynamic system $H(z)$. The graphical representation of this model can be seen in Figure 5.

Hence, when both configurations are combined into a single model with a nonlinear function $f_i(\cdot)$ connected to the input $w(k)$ of the dynamical system $H(z)$ and another nonlinear function $f_o(\cdot)$ to the output $v(k)$ of the dynamical system $H(z)$, the final configuration is the so-called HW model. In this configuration both the input $w(k)$ and output $v(k)$ of the dynamical

Figure 5 – Representation of a Wiener model where the output signal from the dynamic system $v(k)$ is connected to the static nonlinear function $f(\cdot)$ and the input of the dynamic model $v(k)$ is the input of the Winer model $u(k)$.

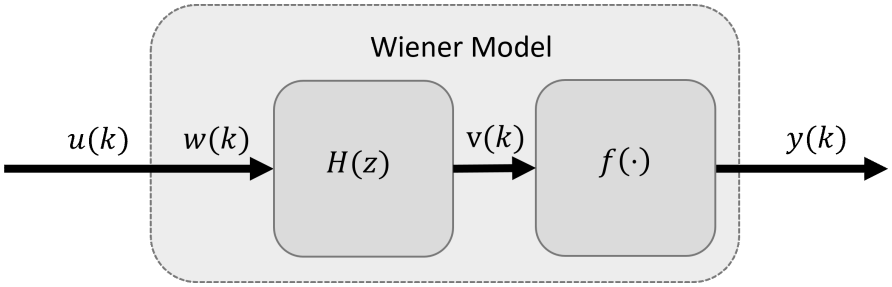

Source: Author.

system are different from the input $u(k)$ and output $y(k)$ of the HW model. The complete structure can be seen in Figure 6.

Figure 6 – Representation of a HW model where the input signal from the dynamic system $w(k)$ is connected to the static nonlinear function $f_i(\cdot)$ and the output of the dynamic model $v(k)$ is connected to the static nonlinear function $f_o(\cdot)$.

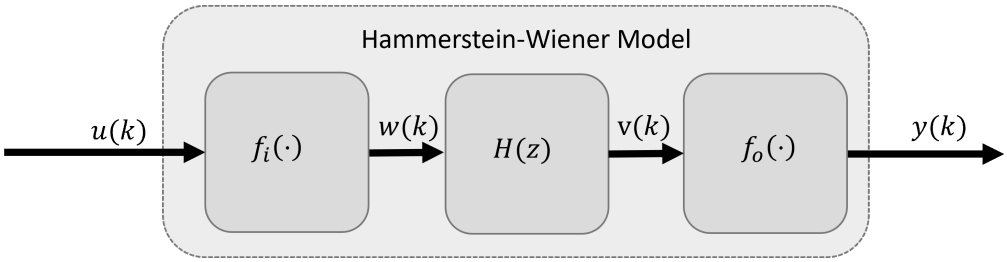

Source: Author.

If instead of the transfer function $H(z)$ it is used a notation of polynomial of regressors as the other models presented, it is possible to define the output $v(k)$ as a function of the input $w(k)$ as the following:

$$v(k) = \frac{B(q)}{F(q)} w(k), \tag{8}$$

where $F(q) \in \mathbb{R}^{N_v \times N_w}$ is the polynomial function of the lag operator applied to the output $v(k) \in \mathbb{R}^{N_v}$ from the linear dynamical system and $B(q) \in \mathbb{R}^{N_v \times N_w}$ the polynomial function of the lag operator applied to the input $w(k) \in \mathbb{R}^{N_w}$. Also, the relation between the input and output of the linear system can be defined as $H(q) \in \mathbb{R}^{N_v \times N_w}$ in the following way:

$$H(q) = \frac{B(q)}{F(q)}. \tag{9}$$

There are several nonlinear static functions that can be used in the HW model for $f_i(\cdot)$ and $f_o(\cdot)$. One of them is the Piecewise Linear PWL. This type of function can be represented in

(10):

$$f(u) = \begin{cases} m_{R1}u, & if \quad 0 \leq u \leq u_{R1}, \\ m_{R2}(u - u_{R1}) + m_{R1}u_{R1}, & if \quad u > u_{R1}, \\ m_{L1}u, & if \quad u_{L1} \leq u < 0, \\ m_{L2}(u - u_{L1}) + m_{L1}u_{L1}, & if \quad u < u_{L1}, \end{cases} \tag{10}$$

in which m_{L2}, m_{L1}, m_{R1} and m_{R2} are the slopes of the linear segments, u_{L1} is a constant for negative inputs and u_{R1} is a constant for positive inputs (TAO; TIAN, 1998).

Figure 7 – Example of a PWL function with $m_{R1} = -2$, $m_{R2} = 4$, $m_{L1} = 6$, $m_{L2} = -4$, $u_{L1} = -4$, and $u_{R1} = 6$.

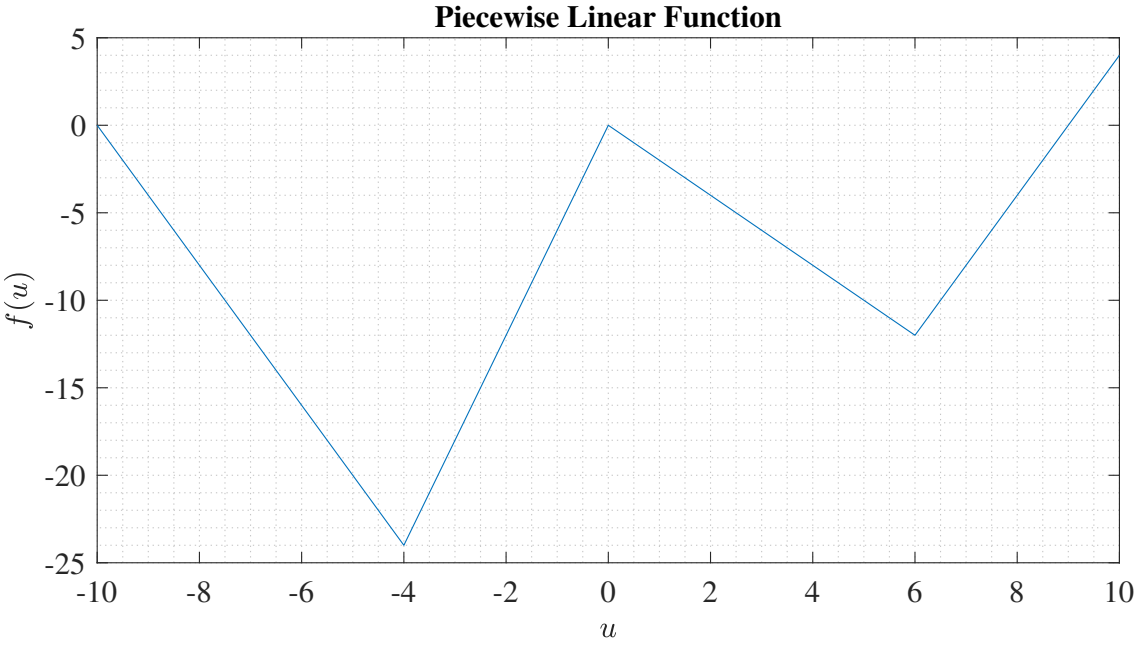

Source: Author.

2.3.3.4 NARX

The Nonlinear Autoregressive with Exogenous Inputs, also known as NARX, is another type of nonlinear model. The NARX model is a variation of ARX that includes nonlinear components (BILLINGS, 2013). The combination of its signals can vary a lot, giving this type of model a high degree of freedom. The polynomial NARX can be described as,

$$\begin{aligned} y(k) = F^l[&y(k-1), \cdots, y(k-n_y), u(k-d), \\ &u(k-d-1), \cdots, u(k-d-n_u)] + e(k), \end{aligned} \tag{11}$$

where $n_y, n_u \in \mathbb{N}$ are the maximum delays for the system's output and input, respectively. Here, $u(k) \in \mathbb{R}^{N_u}$ is the system input, $y(k) \in \mathbb{R}^{N_y}$ is the system output at discrete time $k \in \mathbb{N}$, and $e(k) \in \mathbb{R}^{N_y}$ represents the residue and uncertainties at discrete time k. The function F^l is a nonlinear function of the inputs and output regressors with nonlinearity degree $l \in \mathbb{N}$ and d is the dead-time (BILLINGS, 2013).

2.3.4 Performance Metric

When quantifying the accuracy of a dynamic model, the Mean Square Error (MSE), and Normalized Root Mean Square Error (NRMSE) are used to determine the fitness between the model and collected data (LJUNG, 1999).

$$MSE = \frac{1}{N}\sum_{k=0}^{N-1}\left[p(k) - \hat{p}(k)\right]^2, \tag{12}$$

$$NRMSE = \left\{1 - \sqrt{\frac{\sum_{k=0}^{N-1}(p(k) - \hat{p}(k))^2}{\sum_{k=0}^{N-1}(p(k) - \overline{p})^2}}\right\}100\%, \tag{13}$$

considering

$$\overline{p} = \frac{1}{N}\sum_{k=0}^{N-1} p(k), \tag{14}$$

where $\hat{p}$ is the estimated output from the system, *p(k)* represents the actual value of the variable and N is the number of samples, *k* is the sample number, which varies from 0 to $N-1$.

The performance metric is used to quantify the accuracy. MSE will never be negative since the errors are squared. The value of the error ranges from zero to infinity. MSE increases exponentially with an increase in error. A good model will have a MSE value closer to zero.

NRMSE is a good measure when you want to compare the models of different dependent variables or when the dependent variables are modified (log-transformed or standardized). It overcomes the scale dependency and eases comparison between models of different scales or even between datasets. A model that presents a good fit will have an NRME close to 100%.

Other types of evaluation metrics are used such as Mean Absolute Error (MAE), Mean Bias Error (MBE), Relative Absolute Error (RAE), Mean Absolute Percentage Error (MAPE), Relative Squared Error (RSE), Relative Root Mean Squared Error (RRMSE). These other techniques will not be covered in this work.

2.4 DIGITAL TWIN

Industry and academia define a digital twin in several different ways (TRAUER *et al.*, 2020). For example, according to some, a digital twin is a virtual representation/model that interacts with the physical system throughout its life cycle (GRIEVES; VICKERS, 2017). Other widely circulated definitions regard the need to exchange information between the two spaces involving sensors, data, and models (LEE *et al.*, 2013).

The origin of the Digital Twin is attributed to Michael Grieves and his work with John Vickers of NASA, with Grieves presenting the concept in a lecture on product life-cycle management in 2003 (GLAESSGEN; STARGEL, 2012). In a time when Grieves describes virtual product representations as " . . . relatively new and immature" and data collected about physical products as " . . . limited, manually collected, and mostly paper-based", Grieves and Vickers saw a world where a virtual model of a product would provide the foundations for product life-cycle management.

The initial description defines a Digital Twin as a virtual representation of a physical product containing information about said product, with its origins in the field of product life-cycle management. In an early paper (GLAESSGEN; STARGEL, 2012) Grieves expands on this definition by describing the Digital Twin as consisting of three components, a physical product, a virtual representation of that product, and the bi-directional data connections that feed data from the physical to the virtual representation, and information and processes from the virtual representation to the physical. Grieves depicted this flow as a cycle between the physical and virtual states (mirroring or twinning); of data from the physical to the virtual, and of information and processes from the virtual to the physical. The virtual spaces themselves consisting of any number of sub-spaces that enable specific virtual operations: modelling, testing, optimisation, etc.

Since the inception of the Digital Twin in 2003 the concept has grown in interest, and is now listed by Gartner as a key strategic technology trend for 2019 (PANETTA, 2018). This growth is largely driven by advances in related technologies and initiatives such as Internet-of-Things, big data, multi-physical simulation, and Industry 4.0, real-time sensors and sensor networks, data management, data processing, and a drive towards a data-driven and digital manufacturing future (JONES *et al.*, 2020). As a consequence, both academia and industry have been researching, developing, and seeking to apply Digital Twins or the principles it represents.

This growth has led to inconsistent application and divergence beyond the original descriptions of Greives, leading to a need for consolidation of the concept in light of current research and industry application (JONES *et al.*, 2020).

In this study, a Digital Twin is delineated as the dynamic representation of a physical system, achieved without resorting to direct measurements of the system itself. The Digital Twin furnishes the dynamic behavior of its physical counterpart without necessitating direct measurement; instead, it relies on the estimation of behavior through the utilization of indirect variables. The models comprising the Digital Twin are instantiated within a digital environment, serving as a means for comprehensive study and analysis. In Figure 8 an example of a system with a digital twin is presented.

Figure 8 – Example of a system with a digital twin. Where $u(k)$ is represented as a discrete input of the system, $y(k)$ is the real output of the system, $\hat{y}(k)$ is the digital twin output of the system, and $e(k)$ is the error between the digital twin and the real system.

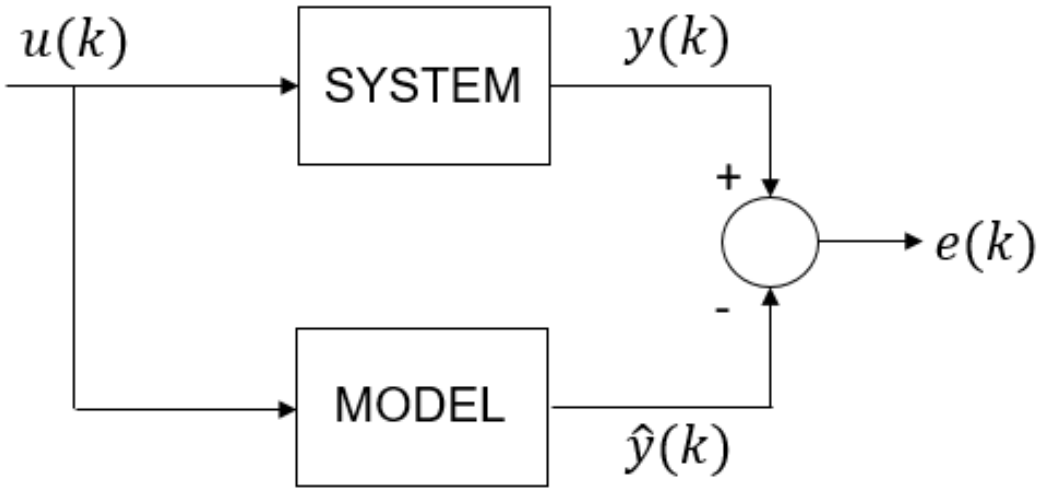

Source: Author.

It is important to note that one practical application of a Digital Twin lies in its association with modeling a system that can be integrated into an embedded system. This model serves various functions, including diagnosis and serving as a foundation for control mechanisms. Achieving such modeling involves the application of system identification concepts, coupled with a deep understanding of the technical intricacies of the twin system. When the system identification process is executed effectively, a Digital Twin of the actual system can be implemented within the embedded software. This digital representation can then be compared to real measurements obtained from the physical system, offering a valuable means of verification and analysis.

2.5 PARTIAL CONSIDERATIONS

This literature review encompasses a comprehensive exploration of crucial elements in the realm of heavy-duty engines, with a particular focus on oil pumps and the utilization of piston cooling jets in diesel engines. Additionally, key concepts in system identification, including ARX models, ARMAX models, Hammerstein-Wiener models, and NARX models, have been elucidated.

Oil Pumps in Heavy-Duty Engines: The section outlines the utilization of oil pumps in diesel engines and underscores their pivotal role in lubricating the system. This specific application has notable implications for both fuel consumption and the overall efficiency of the engine. Consequently, contemporary practices favor the implementation of variable oil pumps over fixed counterparts, as the former allows for electronic control. This adaptability addresses the dynamic requirements of the engine, enabling optimized performance and enhanced efficiency compared to the limitations associated with fixed oil pumps devoid of electronic control.

Piston Cooling Jets in Diesel Engines: In the context of diesel engines, the use of piston cooling jets it is one strategy to manage thermal loads. The literature reveals that piston cooling jets contribute significantly to temperature regulation in diesel engines, preventing overheating and enhancing overall thermal efficiency. The detailed examination of these cooling mechanisms underscores their relevance in the pursuit of improved diesel engine performance and durability.

System Identification and Model Types: The review delves into the realm of system identification, a tool for understanding and modeling complex dynamic systems. Three prominent model types have been explored in the literature:

- **ARX Models (AutoRegressive with eXogenous inputs):** ARX models capture the dynamic behavior of a system by relating the current output to past outputs and inputs. These models provide insights into the system's inherent dynamics and response to external stimuli.

- **ARMAX Models (AutoRegressive Moving Average with eXogenous inputs):** Extending beyond ARX, ARMAX models incorporate a moving average component, offering a more nuanced representation of system dynamics. The inclusion of exogenous inputs enhances the model's predictive capabilities.

- **Hammerstein-Wiener Models:** Hammerstein-Wiener models adopt a nonlinear approach, acknowledging the nonlinearity present in many real-world systems. By combining linear and nonlinear components, these models offer a more faithful representation of complex system behavior.

- **NARX Models (Nonlinear AutoRegressive with eXogenous inputs):** NARX models explicitly embrace nonlinearity, making them adept at capturing intricate relationships within dynamic systems. These models are particularly useful when dealing with systems exhibiting nonlinear behavior.

The forthcoming chapter will delineate the methodology employed in this study and illustrate how the concepts expounded herein were applied. This section aims to elucidate the diverse methodologies employed, showcasing the multifaceted applications of the concepts discussed in the preceding chapters. It will delve into the specific ways in which these theoretical frameworks were operationalized to drive the development and execution of the study.

3 METHODS

The physical system in this study describes the oil system of a heavy-duty diesel engine. It was modeled using real data obtained from a heavy-duty 13-liter turbo diesel engine, equipped with a variable oil pump and a PCJ valve as presented in section 2.2. The relationship between the pressures and voltages applied to each valve was determined by measuring them at different running operating points in torque and engine speed. This means a scenario with different driving conditions for the vehicle. The variables measured for each point are engine rotational speed based on the measurement of the sensor in revolutions per minute, $\omega(k)$, estimated indicated torque of the engine in Nm, $\tau(k)$, OCV duty cycle in percentage, $D_{ocv}(k)$, PCJ valve duty cycle in percentage, $D_{ocv}(k)$, PCJ pressure in kPa, $P_{pcj}(k)$, and main gallery pressure in kPa, $P_{mg}(k)$. The variables were sampled at a variable sampling time, varying from 100 ms to 200 ms. The sampled time of 100 ms was prioritized, but since the protocol used to collect the data has a limitation with regard to the busload, not all variables were able to be sampled at this sampling rate. Therefore, there was the need to increase it to 200 ms for some of them.

Figure 9 – Inputs and outputs of the physical oil system: The oil system receives various inputs, and based on those conditions, the pressure changes in two different measured points. The input variables of the systems are engine rotational speed in revolutions per minute, $\omega(k)$, estimated indicated torque of the engine in Nm, $\tau(k)$, OCV duty cycle in percentage, $D_{ocv}(k)$, and PCJ valve duty cycle in percentage, $D_{pcj}(k)$. The outputs are PCJ pressure in kPa, $P_{pcj}(k)$, and main gallery pressure in kPa, $P_{mg}(k)$.

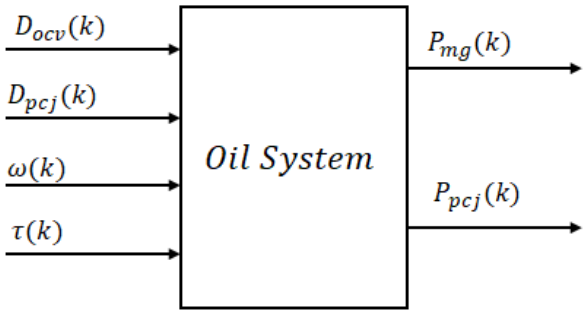

Source: Author.

The Universal Measurement and Calibration Protocol, also known as the XCP was used to collect data from the engine control unit of the vehicle, and the data was resampled at a sampling time of 200 ms. The variables sampled at higher frequencies were downsampled to 200 ms sample time, so all the variables were discretized at the same rate. Hence, the final sampling time for the estimation was 200 ms. Fig. 9 shows the block diagram of the system used in the

study. The inputs of the actual system consist of engine speed, indicated torque, and the duty cycle of the valves, while the outputs are the system's pressures.

Figure 10 – Data from the oil system used in the validation set. All the inputs and outputs of the system are in a time window of 1000 s. Where $\omega(k)$ is the engine speed in revolutions per minute, $\tau(k)$ indicated torque in Nm, $D_{ocv}(k)$ OCV duty cycle in percentage, $D_{pcj}(k)$ PCJ duty cycle in percentage, $Ppcj(k)P_{pcj}(k)$ PCJ pressure in kPa, and $P_{mg}(k)$ the main gallery pressure in kPa.

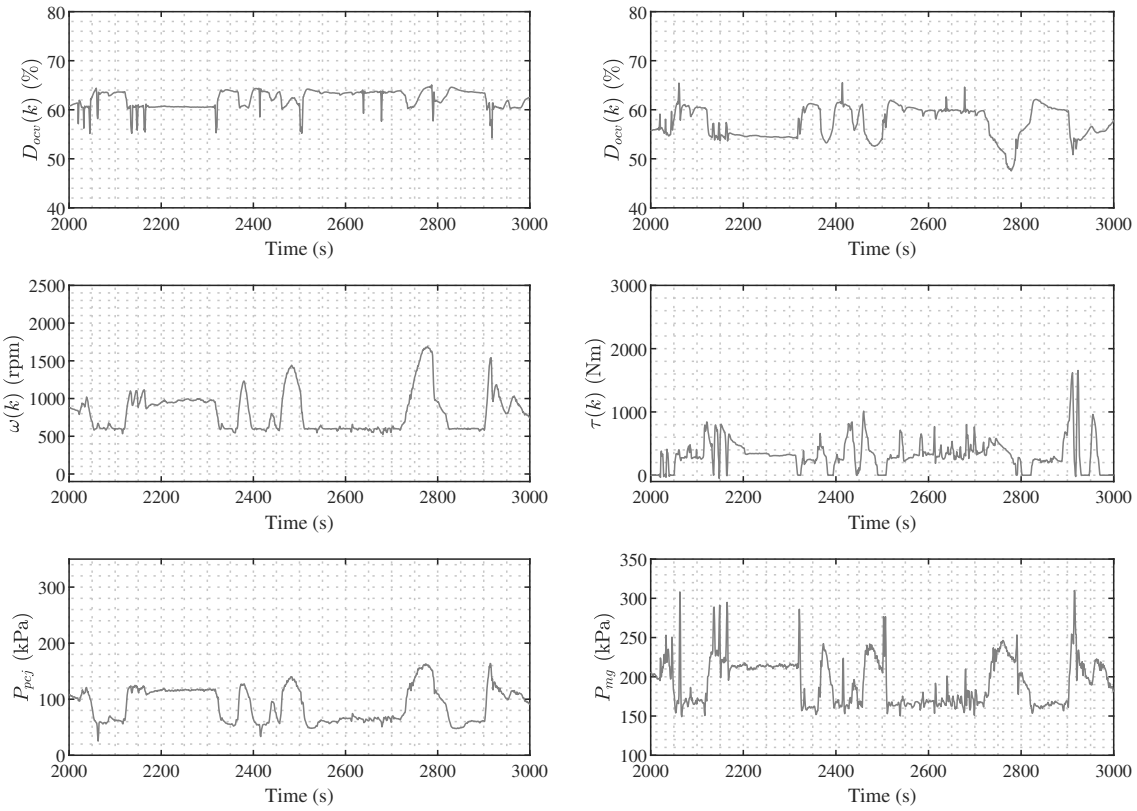

Source: Author.

The dataset was divided into two groups: an estimation set and a validation set. The estimation data consists of 8209 points and the validation group of 3519 points. When adding the samples, the total time of acquisition was close to 40 minutes. The parameters of the model were optimized using 70% of the data, while the remaining 30% was used for validation to check the final model fitness. Since the data represents a time series of a dynamical system, the data was split in a temporal base, using part of the running time as estimation and the other part as validation. The estimation set was used to estimate the model parameters and the validation set was used to test this model against real data and check its fit. An 1000s time window of the validation set can be seen in Fig. 10.

In order to perform the estimation, the system was divided into two different subsystems, which were studied separately. Although the system is a MIMO model, it was split into two

different MISO models. The first MISO used engine speed in revolutions per minute, $\omega(k)$, indicated torque, $\tau(k)$, OCV duty cycle, $D_{ocv}(k)$, PCJ duty cycle, $D_{pcj}(k)$, and PCJ pressure, $P_{pcj}(k)$, as the inputs to estimate the main gallery pressure, $y_1(k)$. The input vector for this model, $u_1(k) \in \mathbb{R}^5$, is defined as

$$u_1(k) = \begin{bmatrix} D_{ocv}(k) \\ D_{pcj}(k) \\ \omega(k) \\ \tau(k) \\ P_{pcj}(k) \end{bmatrix}. \tag{15}$$

The second MISO used engine speed, $\omega(k)$, indicated torque, $\tau(k)$, OCV duty cycle, $D_{ocv}(k)$, PCJ duty cycle, $D_{pcj}(k)$, and main gallery pressure, $P_{mg}(k)$, as the inputs to estimate the PCJ gallery pressure in kPa, $y_2(k)$. The input vector for this model, $u_2(k) \in \mathbb{R}^5$, is defined as

$$u_2(k) = \begin{bmatrix} D_{ocv}(k) \\ D_{pcj}(k) \\ \omega(k) \\ \tau(k) \\ P_{mg}(k) \end{bmatrix}. \tag{16}$$

Since the variables require different models, they were analyzed separately. For each topic, both linear and nonlinear models were evaluated, and the NRMSE for each option was assessed. Both algorithms used are from the Matlab System Identification tool chain. To estimate the parameters of the linear models such as ARX, Matlab uses a QR factorization to solve the least squares estimation problem. For the nonlinear systems, For the nonlinear systems the search algorithm was set to a subspace Gauss-Newton least-squares search. A complete diagram of the two systems can be seen in Figure 11.

The first model analyzed was a linear ARX model. The order selection for the ARX was determined by varying the configuration and assessing the NRMSE of each one during the validation. Different configurations for poles and zeros were tested, but only the combination with the highest NRMSE was used to compare the different models. The transport delay, or input-to-output delay, was set to one sample for all cases. The input-to-output delay was set to one sample so one has a model that can estimate the next step of its state for the next code iteration. Since this is a linear system, the least-squares method was used to estimate the coefficients of this type of model.

Figure 11 – Inputs and outputs of the two MISO systems based on the MIMO system. The first MISO estimates the main gallery pressure in kPa, $y_1(k)$, and the second one the PCJ pressure in kPa, $y_2(k)$. The input variables of the systems are engine rotational speed in revolutions per minute, $\omega(k)$, estimated indicated torque of the engine in Nm, $\tau(k)$, OCV valve duty cycle in percentage, $D_{ocv}(k)$, PCJ valve duty cycle in percentage, $D_{pcj}(k)$, PCJ pressure in kPa, $P_{pcj}(k)$, and main gallery pressure in kPa, $P_{mg}(k)$.

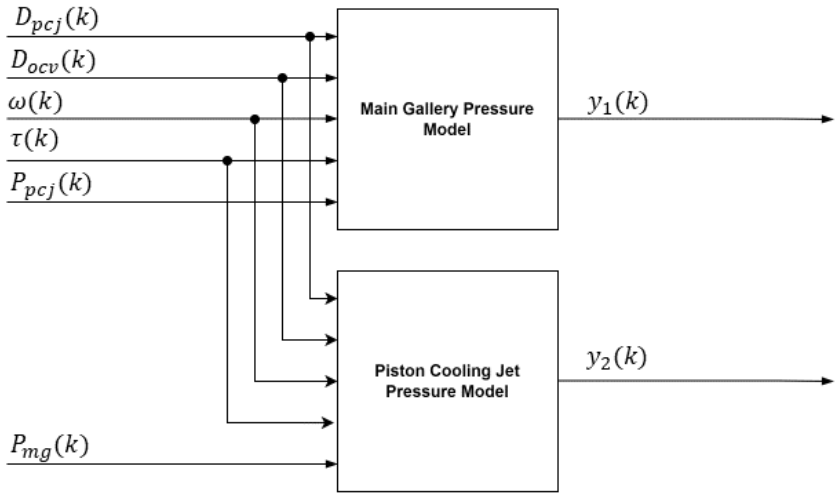

Source: Author.

The second linear model used was an ARMAX, which is a variation of an ARX, but with an additional moving average term. The definition of this model can be seen in (5). The order selection for $A(q)$ and $B(q)$ was the same used for the ARX model. However, the additional noise regressor, $C(q)$, was set to a first-order regressor. The transport delay, or the input-to-output delay, was also set to one sample.

The third model analyzed in this study is a nonlinear HW model, which combines a linear ARX with static nonlinear functions. These functions $f_i(.)$ and $f_o(.)$, shown in the block diagram in Fig. 6, were set to PWL functions with ten breakpoints. The input-to-output delay was also set to one sample in this case.

The last type of model tested was a NARX with a variation of zeros and poles the same way as the other models. The non-linearities explored for the NARX model were defined by employing a linear output function incorporating an offset. In this context, this specific non-linearity involves taking the output of the regressor and subjecting it to a linear function, to which an offset is applied.

The models were determined through the utilization of Matlab scripts. Matlab's built-in functions were employed to compare and estimate parameters across different configurations and conditions. Additionally, the system identification toolbox was utilized, given its integral

role in this analysis. The Matlab version employed for these processes was 2021b.

With regard to the execution of the models to estimate the parameters for each of the models, the following hardware configuration was used:

- **Central Processing Unit (CPU):** Intel Core i7 processor, exemplifying multicore architecture to support intricate computations and concurrent processing;
- **Random Access Memory (RAM):** RAM capacity of 8 GB;
- **Graphics Processing Unit (GPU):** NVIDIA GeForce or Intel Iris Xe Graphics series;
- **Operating Environment:** Operational under Windows 10;
- **Tool Used:** Matlab 2021b;

This hardware configuration served as the foundation for estimating and executing all the models outlined in this study. Additionally, the execution time for each parameter estimation process was meticulously measured and subsequently compared. The timing analysis involved utilizing the dataset for parameter estimation in the models, with the resultant times subjected to thorough comparison.

3.1 PARTIAL CONSIDERATIONS

This methodology delineates the comprehensive approach employed in the execution of this study. Commencing with an elucidation of the data collection procedure, this phase focused on identifying and gathering variables from a vehicle using a serial protocol commonly utilized in automotive applications. Subsequently, the sample times for each variable were normalized to establish a consistent time base.

Following the data collection phase, the study delved into the definition and breakdown of models. This involved a meticulous determination of the number of models, as well as the configurations of inputs and outputs. Additionally, the dataset was partitioned into validation and estimation sets. The estimation set was utilized for parameter estimation of a specific model, while the validation set served as a means to assess the behavior of the estimated model.

Within this section, a detailed presentation was made regarding the configuration of both linear and nonlinear models, elucidating the considerations that influenced their establishment during the course of the study. Notably, the configurations of these models varied in terms of

the number of poles and zeros, adhering to the mathematical conditions outlined in the previous section.

Concluding the methodology, the hardware configuration employed for model estimation was explicated, providing insights into the tools and equipment utilized in the practical implementation of the study.

4 RESULTS AND DISCUSSION

The results will be presented in two subsections. The first subsection will describe the estimates of the main gallery pressure, while the second subsection will focus on the estimates of the PCJ pressure. The model with the highest NRMSE is presented at the end of each subsection.

4.1 MAIN GALLERY PRESSURE

The results for the estimation of the parameters are exhibited based on the two best models selected and the two worst models compared against the validation set for each configuration. The validation set was used to check if the parameters estimated during the estimation of the parameters for that specific model can reflect the behavior of the remaining points of data as discussed in the previous section.

By varying the configuration of the ARX model across a range from 1 to 4 for both zeros and poles, it was identified the most suitable model as the ARX model, characterized by a third-order $A(q)$ as defined in Equation (3) and a fourth-order $B(q)$. Conversely, the least effective ARX model consisted of a first-order $A(q)$ and a fourth-order $B(q)$. The characteristics of the zeros are presented in vector notation, following the conventions introduced in 15. The results regarding the model against the validation set are presented in Table 1. The column representing the poles is shown in a vector form, where each of its positions corresponds to the number of poles of one of the inputs. The vector of inputs can be checked in the previous section in Equation (15). Also, in this table, the column regarding the execution time shows the time in seconds that the hardware took to estimate the parameters of the model.

When incorporating an additional term to create an ARMAX model with a first-order $C(q)$, the outcomes exhibited a small variation in the dynamic behavior compared to the ARX model. The poorest-performing ARMAX model failed to adequately capture the system dynamics using the validation data, resulting in a model that could not represent the real data at all. As a result, the NRMSE for these models was recorded with a high magnitude negative number, represented as $-\infty$, when running the model with the parameters estimated with the training set against the data from the validation set. Just noting that the best possible NRMSE is a value close to 100 %. Conversely, the most proficient ARMAX model exhibited a 2% enhancement in NRMSE compared to the best ARX.

Table 1 – Linear Models validation results for main gallery pressure using the parameters estimated in the parameter estimation phase.

Model	Poles	Zeros	Moving Average Order	NRMSE	Execution Time
ARX	3	[4,1,3,3,1]	NA	74.70%	0.19 s
ARX	3	[4,1,4,3,1]	NA	74.67%	0.36 s
ARX	1	[1,3,1,4,1]	NA	56.19%	0.24 s
ARX	1	[1,3,1,1,1]	NA	56.28%	0.17 s
ARMAX	3	[4,3,4,1,4]	1	76.63%	0.78 s
ARMAX	1	[3,4,2,4,2]	1	76.60%	0.71 s
ARMAX	3	[2,2,3,4,3]	1	$-\infty$	1.44 s
ARMAX	1	[2,4,4,4,4]	1	$-\infty$	0.95 s

Source: Author.

The worst configurations for the models against the validation set were raised to show that when running those models during the parameters estimation high NRMSE results were presented. The results for those models during the parameter estimation phase can be seen in Table 2. That gives the notion that the models can find a combination to describe the system dynamics when estimating the parameters, but they were not able to generalize the model for different conditions. Here, the validation set and estimation set is from the same system, however, it was operating in a different region.

Table 2 – Results for linear models in the parameters estimation phase. The results presented in this table were returned by the training algorithm during using the dataset used in this specific phase.

Model	Poles	Zeros	Moving Average Order	MSE	FPE	NRMSE
ARX	3	[4, 1, 3, 3, 1]	NA	21.89	21.99%	85.14%
ARX	3	[4, 1, 4, 3, 1]	NA	21.24	21.35%	85.36%
ARX	1	[1, 3, 1, 4, 1]	NA	39.95	40.10%	79.92%
ARX	1	[1, 3, 1, 1, 1]	NA	42.57	42.69%	79.27%
ARMAX	3	[4, 3, 4, 1, 4]	1	23.51	23.65%	84.60%
ARMAX	1	[3, 4, 2, 4, 2]	1	54.37	54.65%	76.57%
ARMAX	3	[2, 2, 3, 4, 3]	1	28.69	28.85%	82.98%
ARMAX	1	[2, 4, 4, 4, 4]	1	29.22	29.39%	82.83%

Source: Author.

Figure 12 visually compares the two top-performing models. Notably, both linear models achieved accurate estimations under conditions where the pressure derivative is not so high. Also, during more aggressive transient conditions, the behavior of the two models presented a similar behavior, showing a high NRMSE to describe the system's dynamics under those conditions. The final best result achieved was from the ARMAX model with a third-order

$A(q)$, a fourth-order $B(q)$, and a first-order moving average term, $C(q)$, with a NRMSE of 76.63%.

Figure 12 – Measured pressure signal in the validation dataset for main gallery pressure $P_{mg}(k)$ against the ARX an ARMAX models' output $y_1(k)$ in a 500 s time window with sampling time of 200 ms.

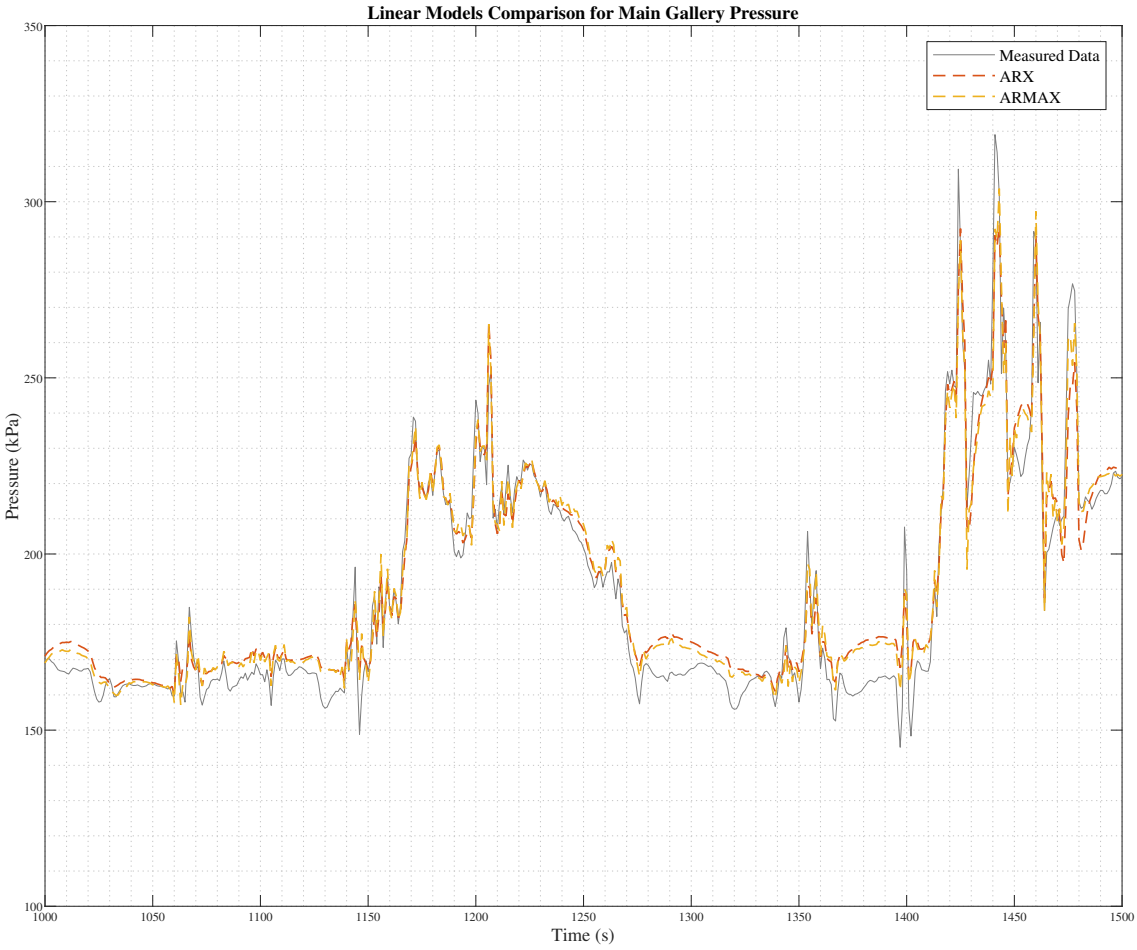

Source: Author.

When testing the nonlinear models, a better result was achieved compared to the linear ones. The HW model was set to 5, 10, 14, 18 nonlinear PWL for the inputs with the same configuration for the output, and a linear model varing the number of poles and zeros from 1 to 4 were tested. The best performing model used a 5 nonlinear PWL with four poles and three zeros. The Final Prediction Error (FPE) for this model was 18.27%, and the MSE 17.85 for the estimation set. The final NRMSE achieved in the validation set was 84.86%. The model described here comprises a fourth-order $A(q)$ and a third-order $B(q)$. Also, by looking at FPE and MSE it is possible to see that the model could show a good estimate in both training and validation sets. Table 3 consolidates the results from the best and worst nonlinear models tested using the parameters estimated in the estimation phase using the estimation set against the validation data.

Table 3 – Nonlinear Models validation results for main gallery pressure using the parameters estimated in the parameter estimation phase.

Model	Poles	Zeros	Nonlinearity	NRMSE	Execution Time
HW	4	$[2, 3, 1, 2, 1]$	5 PWL	84.86%	5.34 s
HW	4	$[3, 2, 2, 3, 3]$	10 PWL	84.67%	6.68 s
HW	1	$[3, 4, 3, 2, 1]$	10 PWL	$-\infty$	4.74 s
HW	1	[3,1,1,3,4]	10 PWL	$-\infty$	7.42 s
NARX	3	$[4, 1, 4, 3, 1]$	Linear Function and Offset	75.54%	0.47 s
NARX	3	$[4, 1, 4, 4, 1]$	Linear Function and Offset	75.52%	0.44 s
NARX	1	$[2, 4, 1, 4, 1]$	Linear Function and Offset	58.82%	0.45 s
NARX	1	$[2, 4, 1, 3, 1]$	Linear Function and Offset	58.86%	1.06 s

Source: Author.

Also, it is good to take note why the worst models were presented. Table 4 shows the values during the estimation set. Here it is possible to check that during the training of the parameters the results are a bit different from validation. Here, it is shown that depending on the selection of the nonlinear model, the representation can diverge in a high degree from the real data. This is shown by the high values of MSE and FPE presented by those models. That was only seen in the HW models and it did no occur for the NARX models.

Table 4 – Results for nonlinear models in the parameters estimation phase. The results presented in this table were returned by the training algorithm during using the dataset used in this specific phase.

Model	Poles	Zeros	Nonlinearity	MSE	FPE	NRMSE
HW	4	$[3, 2, 2, 3, 3]$	5 PWL	17.85	18.27%	86.58%
HW	3	$[1, 3, 3, 4, 2]$	10 PWL	24.51	25.46%	84.27%
HW	1	$[3, 4, 3, 2, 1]$	10 PWL	289.70	300.12	45.93%
HW	1	$[3, 1, 1, 3, 4]$	10 PWL	368.62	381.79	39.01%
NARX	3	$[4, 1, 4, 3, 1]$	Linear Function with Offset	20.91	21.00%	85.47%
NARX	3	$[4, 1, 4, 4, 1]$	Linear Function with Offset	20.88	20.98%	85.48%
NARX	1	$[2, 4, 1, 4, 1]$	Linear Function with Offset	29.97	30.09%	82.61%
NARX	1	$[2, 4, 1, 3, 1]$	Linear Function with Offset	30.08	30.19%	82.57%

Source: Author.

The NARX model presented an FPE of 21.00% and an MSE of 20.91 in the estimation set. The NRMSE for this model was similar to the linear ARMAX model and presented almost 10.00% worse NRMSE than the HW model. The NARX model with the best configuration found was composed of a third-order $A(q)$, fourth-order $B(q)$, and 1 sample input-output delay. The nonlinearity used for the this model was a simple linear function with an offset for the output of the regressors. The overall NRMSE achieved for this model was 75.54%. Also, here it is good to notice that even the worst combination found was able to describe the model and find

a set of parameters to represent the dynamics. This shows that even a low-order model is able to generalize the dynamics of the system even with low NRMSE when compared to the other configurations. Fig. 13 shows a comparison between the two nonlinear models.

Figure 13 – Measured pressure signal in the validation dataset for main gallery pressure $P_{mg}(k)$ against the HW and NARX models' output $y_1(k)$ in a 500 seconds time window.

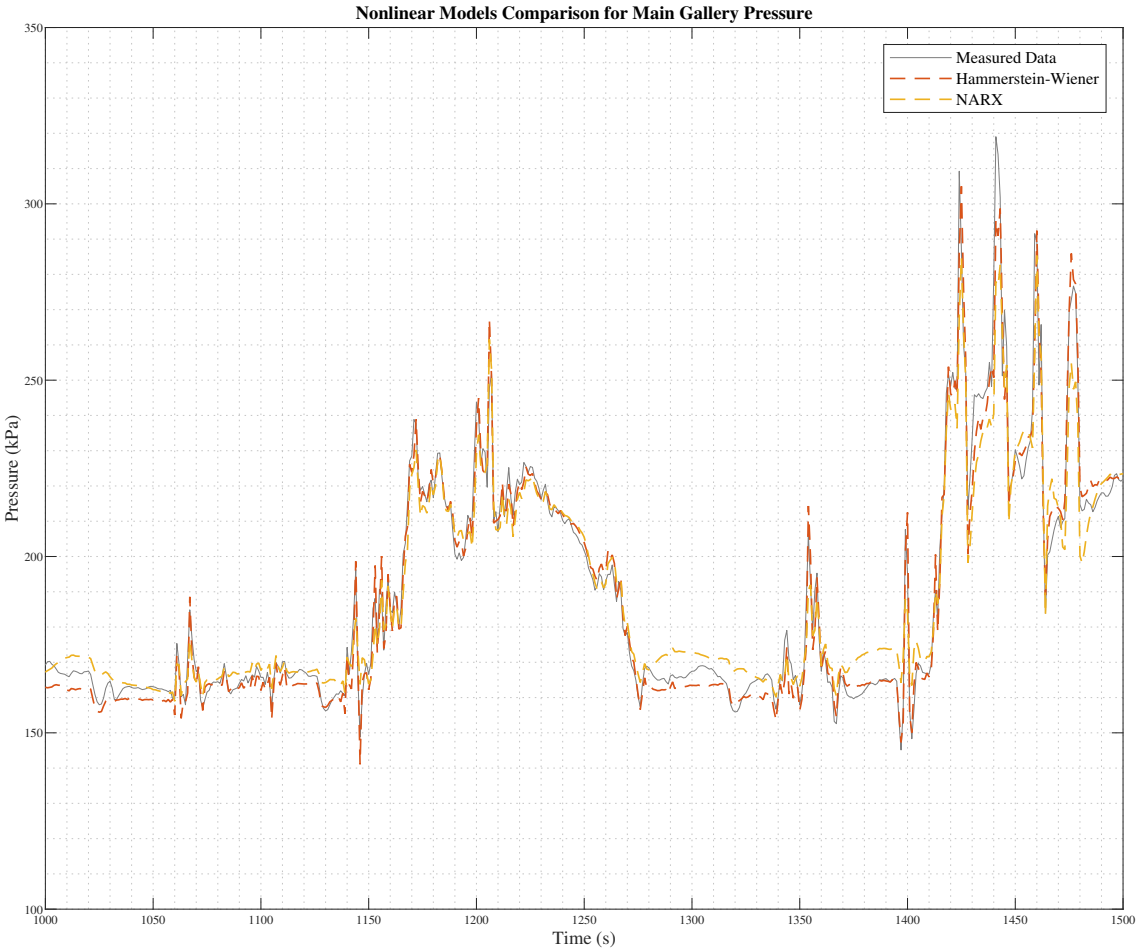

Source: Author.

Using the notation described in section 3, the nonlinear functions for the HW model with the best fit can be seen in Fig. 14. The resulting equations for $F(q)$ and $B(q)$ are presented in (17) to (26).

$$F_1(q) = 1 - 0.599q^{-1} - 0.860q^{-2} + 0.483q^{-3}, \tag{17}$$

$$F_2(q) = 1 - 0.982q^{-1} + 0.279q^{-2}, \tag{18}$$

$$F_3(q) = 1 - 1.586q^{-1} + 0.589q^{-2}, \tag{19}$$

$$F_4(q) = 1 - 2.617q^{-1} + 2.400q^{-2} - 0.782q^{-3}, \tag{20}$$

$$F_5(q) = 1 - 2.160q^{-1} + 1.324q^{-2} - 0.164q^{-3}, \tag{21}$$

$$B_1(q) = q^{-1} - 0.402q^{-2} - 0.832q^{-3} + 0.267q^{-4}, \tag{22}$$

$$B_2(q) = 0.302q^{-1} + q^{-2} - 0.444q^{-3} - 0.165q^{-4}, \tag{23}$$

$$B_3(q) = -0.448q^{-1} + q^{-2} - 0.693q^{-3} + 0.142q^{-4}, \tag{24}$$

$$B_4(q) = -1.038q^{-1} + 1.531q^{-2} + q^{-3} - 1.489q^{-4}, \tag{25}$$

$$B_5(q) = -0.351q^{-1} - 0.024q^{-2} + q^{-3} - 0.674q^{-4}. \tag{26}$$

Figure 14 – Nonlinear functions $f_i(\cdot)$ and $f_o(\cdot)$ for $y_1(k)$. Where $f_i(\cdot)$:$\mathbb{R}^5 \rightarrow \mathbb{R}^5$ composed by $\omega(k)$, engine speed in revolutions per minute, $\tau(k)$ indicated torque in Newton-metre, $D_{ocv}(k)$ OCV duty cycle in percentage, $D_{pcj}(k)$ PCJ duty cycle in percentage, $P_{pcj}(k)$ PCJ pressure in Kilopascal. $f_o(\cdot)$:$\mathbb{R} \rightarrow \mathbb{R}$ is the nonlinearity relation between the estimated main gallery pressure, $y_1(k)$, and the output of the linear system $x_1(k)$.

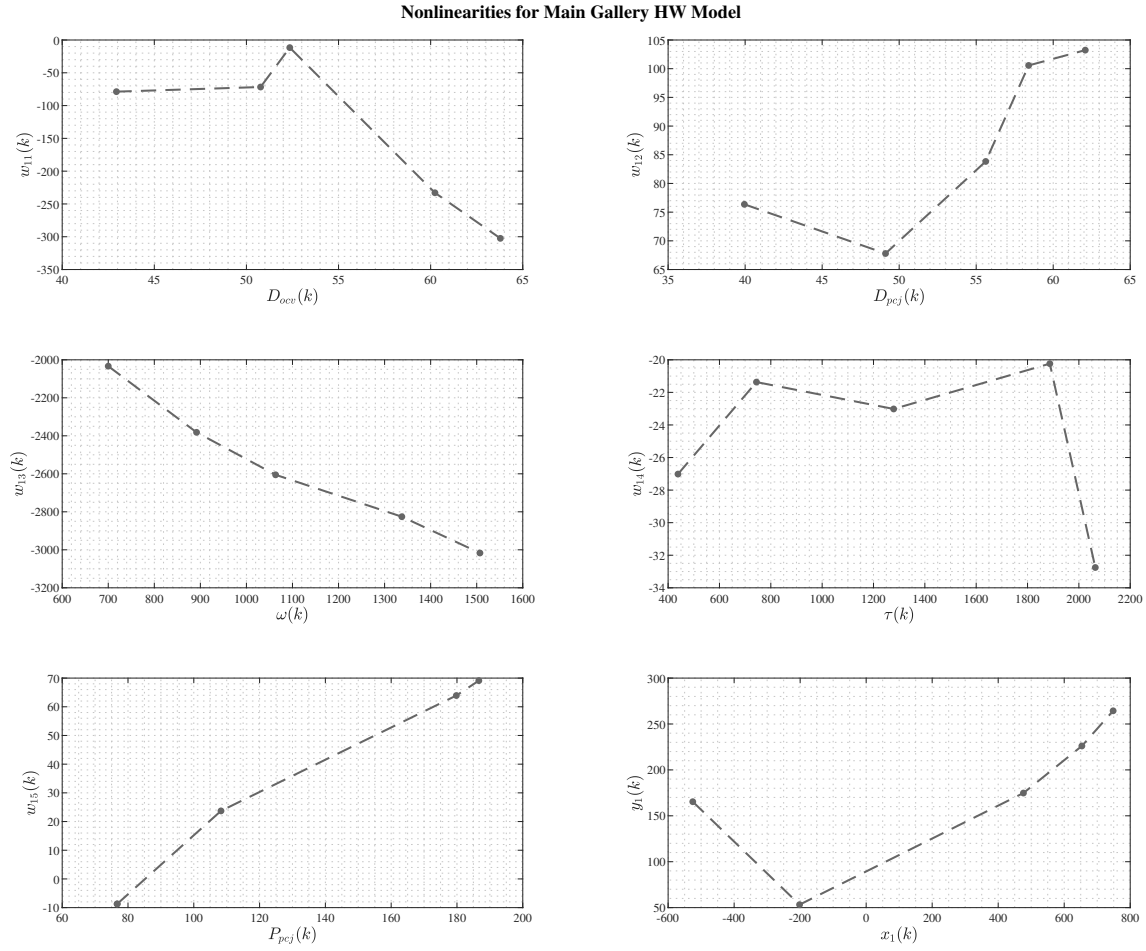

Source: Author.

In summary, one can see that the ARMAX model demonstrated better results in describing the system compared to the ARX. Hence, the NRMSE value of the ARMAX model was 2% greater than that of the ARX model. When adding the nonlinear component to the ARX model, no increase in NRMSE was observed. The final HW model exhibited the best overall NRMSE, which was approximately 10% higher than that of the linear ARX model. This is possibly due to the type of nonlinearity used. Since for the NARX model only a linear function with offset was used. It can be noticed that the difference between the models was greater for models that can better describe the transient behavior in low-pressure points. This can be seen in the data comparison shown in Figures 12 and 13.

The most significant difference between the models is apparent in their transient behavior. However, this discrepancy arises due to transitions between different operating points. Essentially, the system's nonlinearities in inputs and outputs result in distinct behaviors depending on the region. As the system's inputs shift from one region to another, this variation becomes more pronounced. Consequently, nonlinear models excel in addressing the intricacies of transient behavior, providing a more faithful reflection of the system's response during dynamic phases.

Conversely, if the transient dynamics do not necessitate such high precision and fidelity, simpler linear models like ARX or ARMAX can suffice in describing the system's behavior adequately. Given that the distinction between ARX and ARMAX models is relatively modest, opting for an ARX model provides a pragmatic solution. The advantages of simplicity in implementation and a reduced risk of overfitting make the ARX model a fitting choice for scenarios where a comprehensive representation of transient dynamics is not imperative.

4.2 PCJ PRESSURE

To estimate the PCJ model, a similar approach to the primary gallery pressure estimation was employed. Just as in the previous models, both linear and nonlinear variants were explored, with variations in the number of zeros and poles ranging from 1 to 4. To evaluate model performance, the best and worst results were systematically compared.

For the linear models, utilizing both the ARX and ARMAX configurations, various settings and combinations were examined. The specific configurations for these linear models are detailed in Table 5. The values presented are comparing the models with the parameters estimated agains the validation set. This comprehensive analysis allowed one can see insights into the efficacy of different model setups in replicating the PCJ's behavior accurately. The

configuration for all ARMAX models presented was by using a first order moving average term.

Table 5 – Linear Models validation results for PCJ gallery pressure using the parameters estimated in the parameter estimation phase.

Model	Poles	Zeros	Moving Average Order	NRMSE	Execution Time
ARX	2	$[4, 1, 4, 2, 2]$	NA	78.51%	0.12 s
ARX	4	$[4, 1, 3, 2, 2]$	NA	78.51%	0.11 s
ARX	4	$[1, 4, 2, 1, 1]$	NA	$-\infty$	0.13 s
ARX	2	$[1, 4, 2, 1, 1]$	NA	$-\infty$	0.12 s
ARMAX	4	$[4, 4, 3, 3, 1]$	1	83.12%	1.13 s
ARMAX	1	$[2, 3, 3, 3, 3]$	1	82.96%	0.79 s
ARMAX	2	$[2, 4, 3, 4, 4]$	1	$-\infty$	1.49 s
ARMAX	2	$[3, 1, 3, 3, 3]$	1	$-\infty$	0.41 s

Source: Author.

When estimating the parameters, the results presented by each of the configurations were a bit different. The results from the estimation phase can be seen in Table 6. Here, it is possible to see that even models with a low NRMSE when compared to the validation set presented a high NRMSE. This indicates that the parameter estimation found a set of parameters that represents the dynamics of the system, but this model was not able to generalize the system‘s behavior with that high NRMSE value.

Table 6 – Results for linear models in the parameters estimation phase. The results presented in this table were returned by the training algorithm during using the dataset used in this specific phase.

Model	Poles	Zeros	Moving Average Order	MSE	FPE	NRMSE
ARX	2	$[4, 1, 4, 2, 2]$	NA	4.84	4.86%	91.99%
ARX	4	$[4, 1, 3, 2, 2]$	NA	4.80	4.82%	92.04%
ARX	4	$[1, 4, 2, 1, 1]$	NA	4.91	4.93%	91.80%
ARX	2	$[1, 4, 2, 1, 1]$	NA	4.99	5.01%	91.89%
ARMAX	4	$[4, 4, 3, 3, 1]$	1	3.84	3.86%	92.88%
ARMAX	1	$[2, 3, 3, 3, 3]$	1	4.45	4.47%	92.33%
ARMAX	2	$[2, 4, 3, 4, 4]$	1	11.84	11.91%	87.50%
ARMAX	2	$[3, 1, 3, 3, 3]$	1	11.97	12.02%	87.43%

Source: Author.

The ARMAX model emerged as the top-performing linear model for PCJ pressure estimation, outshining the best ARX model by a notable margin, boasting a 5% lower NRMSE. It is worth highlighting a distinction from the main gallery pressure estimation. In this case, while both ARX and ARMAX models yielded promising combinations during the training phase using the estimation set, the subsequent validation set revealed a significant drop in their ability to represent the system accurately. This phenomenon signals a clear case of model overfitting,

wherein the model becomes excessively tailored to the training data, impeding its capacity to generalize and capture the system's dynamics effectively. In Figure 15 the two models are compared against the validation data. There one can see that the behavior of these two models is similar; however, at some points of higher pressure, the ARMAX model showed a better fit to the data. The best model was composed of a fourth-order $A(q)$ and fourth-order $B(q)$ ARMAX model with a first order moving average term, $C(q)$.

Figure 15 – Measured pressure signal in the validation dataset for PCJ gallery pressure $P_{pcj}(k)$ against the ARX an ARMAX models' output, $y_2(k)$, in a 500 seconds time window.

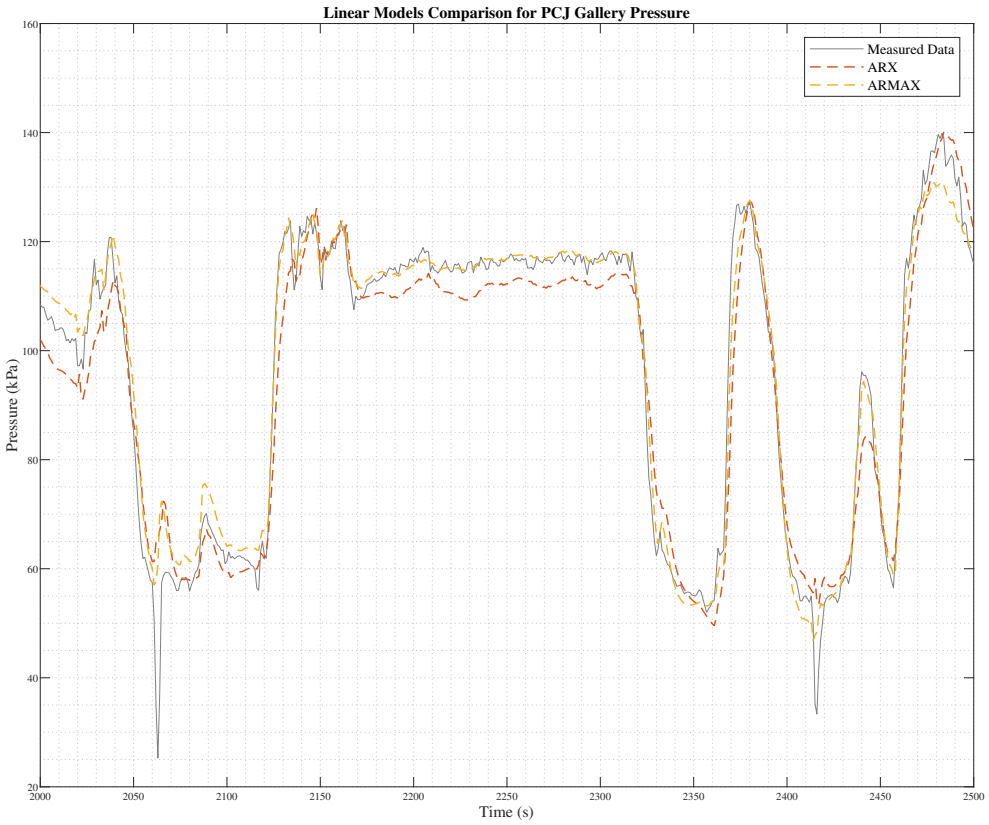

Source: Author.

In contrast to the linear models, the nonlinear models demonstrated notably improved performance. The standout performer among these nonlinear models was the HW model, boasting an impressively high NRMSE of 89.71%. This achievement represented a substantial 6% higher NRMSE when compared to both the best NARX model that presented a NRMSE of 83.95% and the top-performing linear model that presented a NRMSE of 92.88%. When compared the best NARX model to the best ARMAX model, it is observed that the disparity in NRMSE was not as pronounced. However, an essential observation is that the NARX model, even in its least favorable combinations, managed to find a suitable generalization for the system. This stands in

contrast to the HW model, in which the least effective configurations struggled to describe the system's dynamics comprehensively, emphasizing the robustness and flexibility of the NARX approach. The summary of results using the estimation set to estimate the parameters of the model and this model agains the validation set are shown in Table 7.

Table 7 – Nonlinear Models validation results for PCJ gallery pressure using the parameters estimated in the parameter estimation phase.

Model	Poles	Zeros	Nonlinearity	NRMSE	Execution Time
HW	4	$[3, 4, 4, 4, 4]$	5 PWL	89.76%	4.18 s
HW	4	$[1, 2, 4, 2, 1]$	5 PWL	89.72%	4.79 s
HW	1	$[1, 1, 2, 1, 4]$	10 PWL	58.08%	6.21 s
HW	1	$[4, 1, 2, 2, 1]$	10 PWL	$-\infty$	5.06 s
NARX	4	$[2, 1, 4, 2, 1]$	Linear Function and Offset	83.95%	0.22 s
NARX	3	$[2, 1, 4, 2, 1]$	Linear Function and Offset	83.92%	0.20 s
NARX	1	$[1, 4, 1, 1, 1]$	Linear Function and Offset	63.43%	0.42 s
NARX	1	$[1, 4, 1, 2, 1]$	Linear Function and Offset	64.05%	0.20 s

Source: Author.

The worst models were brought up to show that even that models that presented a high NRMSE during the training of the parameters could not present the same results against the validation set. The concatenated data for the training set are summarized in Table 8.

Table 8 – Results for nonlinear models in the parameters estimation phase. The results presented in this table were returned by the training algorithm during using the dataset used in this specific phase.

Model	Poles	Zeros	Nonlinearity	MSE	FPE	NRMSE
HW	4	$[3, 4, 4, 4, 4]$	5 PWL	9.82	10.08%	88.61%
HW	4	$[1, 2, 4, 2, 1]$	5 PWL	6.59	6.75%	90.67%
HW	1	$[1, 1, 2, 1, 4]$	10 PWL	145.29	150.37	56.21%
HW	1	$[4, 1, 2, 2, 1]$	10 PWL	364.82	377.67	30.61%
NARX	4	$[2, 1, 4, 2, 1]$	Linear Function and Offset	4.49	4.51%	92.30%
NARX	3	$[2, 1, 4, 2, 1]$	Linear Function and Offset	4.50	4.52%	92.29%s
NARX	1	$[1, 4, 1, 1, 1]$	Linear Function and Offset	5.35	5.37%	91.59%
NARX	1	$[1, 4, 1, 2, 1]$	Linear Function and Offset	5.34	5.36%	91.60%

Source: Author.

In Figure 16 it is shown that both HW and NARX models can better represent the pressure behavior even in higher pressure values. When comparing the results from Figure 16 and Figure 15 shows that the main difference is within higher pressure values. Also, the high drops in pressure were captured by the HW model, what it is not the case for all other model representations.

Figure 16 – Measured pressure signal in the validation dataset for PCJ gallery pressure $P_{pcj}(k)$ against the HW a NARX models' output $y_2(k)$ in a 500 seconds time window.

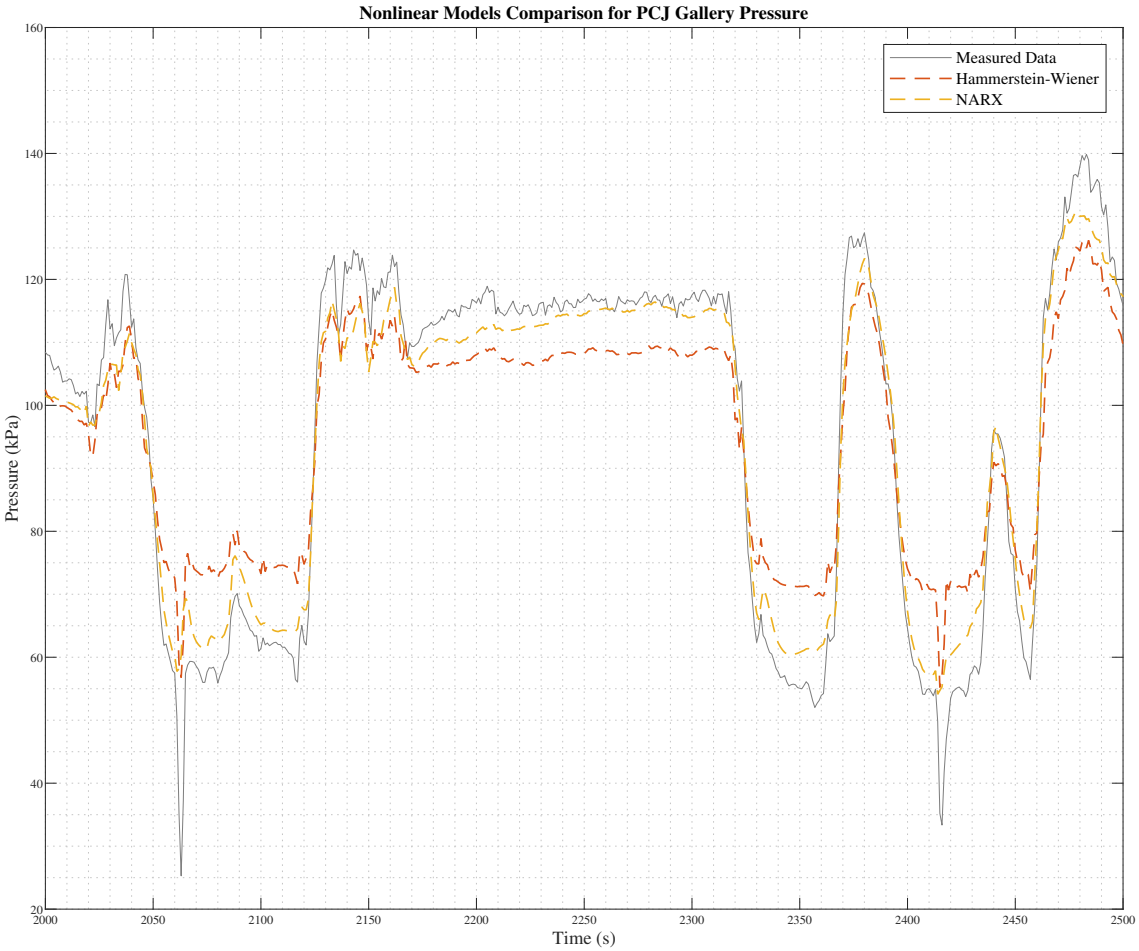

Source: Source:Author.

Using the notation described in section 3, the nonlinear functions for the HW model with the best fit can be seen in Fig. 17. The resulting equations for $F(q)$ and $B(q)$ are in (27) to (36).

Figure 17 – Nonlinear functions $f_i(\cdot)$ and $f_o(\cdot)$ for $y_2(k)$. Where $f_i(\cdot)$:$\mathbb{R}^5 \rightarrow \mathbb{R}^5$ composed by $\omega(k)$, engine speed in revolutions per minute, $\tau(k)$ indicated torque in Nm, $D_{ocv}(k)$ OCV duty cycle in percentage, $D_{pcj}(k)$ PCJ duty cycle in percentage, $P_{mg}(k)$ main gallery pressure in kPa. $f_o(\cdot)$: $\mathbb{R} \rightarrow \mathbb{R}$ is the nonlinearity relation between the estimated PCJ gallery pressure, $y_2(k)$, and the output of the linear system $x_2(k)$.

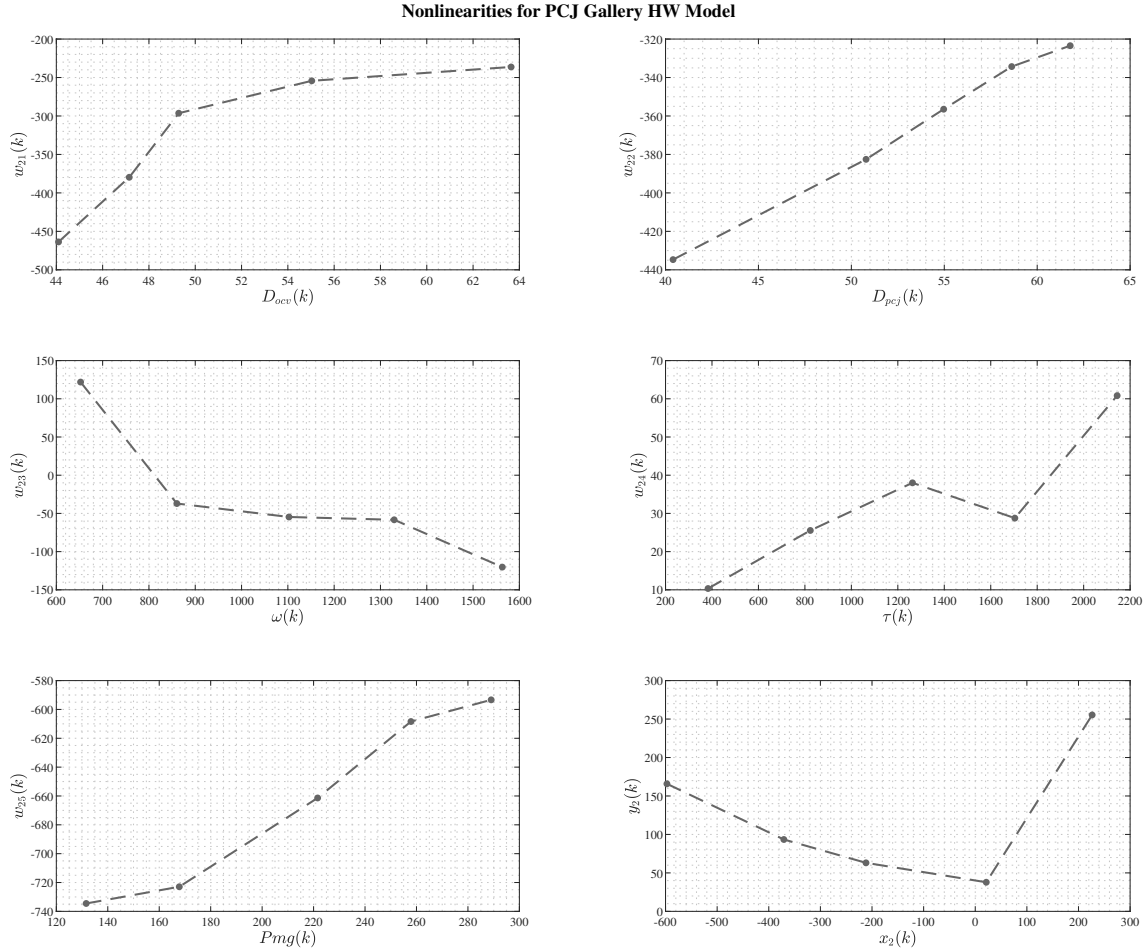

Source: Author.

$$F_1(q) = 1 - 1.227q^{-1} + 0.027q^{-2} + 0.201q^{-3}, \tag{27}$$

$$F_2(q) = 1 - 0.949q^{-1} + 0.113q^{-2} - 0.555q^{-3} + 0.396q^{-4}, \tag{28}$$

$$F_3(q) = 1 - 0.955q^{-1} - 0.388q^{-2} + 0.344q^{-3} - 0.005q^{-4}, \tag{29}$$

$$F_4(q) = 1 - 2.453q^{-1} + 1.645q^{-2} + 0.071q^{-3} - 0.263q^{-4}, \tag{30}$$

$$F_5(q) = 1 - 0.356q^{-1} - 1.158q^{-2} + 0.359q^{-3} - 0.163q^{-4}, \tag{31}$$

$$B_1(q) = -0.720q^{-1} + q^{-2} - 0.294q^{-3} - 0.016q^{-4}, \tag{32}$$

$$B_2(q) = -2.958q^{-1} + q^{-2} - 0.160q^{-3} + 2.063q^{-4}, \tag{33}$$

$$B_3(q) = -0.628q^{-1} + q^{-2} + 0.254q^{-3} - 0.117q^{-4}, \tag{34}$$

$$B_4(q) = -0.321q^{-1} + -0.981q^{-2} + q^{-3} - 0.340q^{-4}, \tag{35}$$

$$B_5(q) = q^{-1} - 0.278q^{-2} - 1.002q^{-3} - 0.276q^{-4}. \tag{36}$$

4.3 DISCUSSION

After scrutinizing the results, it is evident that both systems exhibited a normalized root mean square error (NRMSE) greater than 75% across all model types. The employment of nonlinear models appeared more suitable for both systems, indicating a potential nonlinearity associated with the inputs and outputs. This suggests the presence of nonlinearities within these systems, implying that the impact of certain inputs and the effects of outputs vary depending on the operating region.

For the estimation of main gallery pressure, the most suitable linear model was the ARMAX model, with only a marginal difference compared to the ARX model. Although the ARX model displayed superior results in NRMSE during the training phase, it struggled to generalize as effectively as the ARMAX model, as evidenced by its performance on the validation set.

Among the nonlinear models for main gallery pressure estimation, the HW model outperformed all others in both training and validation phases. Notably, increasing the number of breakpoints in a piecewise-linear (PWL) function did not lead to a corresponding increase in NRMSE. Moreover, a simpler HW model with fewer breakpoints exhibited shorter execution times during training compared to configurations with more breakpoints, but the same number of poles. While the NARX model yielded superior results to linear models, it fell short of achieving the performance demonstrated by the HW model, likely due to the simplicity of the linear function employed in its output.

Turning attention to PCJ pressure estimation, the results mirrored those of the main gallery, albeit with a higher NRMSE across all configurations. This discrepancy may be attributed to the mechanical linkage between the oil galleries, particularly the direct connection between

the PCJ and main gallery pressures. Linear models, specifically the ARMAX model, exhibited optimal performance during the training phase with a NRMSE of almost 92% and an 83.12% NRMSE during validation. This outcome surpassed the results for main gallery estimation by 7.00%, potentially due to the mechanical linkage between the galleries and the use of main gallery pressure as input to PCJ pressure model.

Among the nonlinear models for PCJ pressure estimation, the HW model again emerged as the top performer. During parameter training, the NARX model initially outperformed the HW model. However, when assessing results against the validation set, the HW model exhibited a 6.00% improvement. Additionally, the optimal number of breakpoints for PWL in the HW models was identified as 5, with an increase in this parameter not resulting in an escalation of NRMSE.

5 CONCLUSION

This work evaluates some dynamic empirical models of an oil system that is applied to a turbo diesel engine. To achieve this, data was collected from a real-world application, and the models' parameters were estimated and validated using this dataset. Several models were tested to identify the one that best describes the behavior of this dynamic system.

The main result of the study is the estimation of the main gallery pressure and PCJ gallery pressure using a HW model with a PWL function. The model for main gallery pressure presented an NRMSE of 84.86%. The worst-performing model for the same system when comparing the best model configuration for each type was the ARX model, with an NRMSE of 74.70%. Similar results were observed for the PCJ pressure estimation, with the HW model outperforming the other models with an NRMSE of 89.76%, and the worst model being the linear ARX model with an NRMSE of 78.51%. Both linear and nonlinear combinations were able to achieve a NRMSE higher than 70% for both systems. For the PCJ pressure estimation the results were even better showing that even the worst configuration tested presented a NRMSE higher than 85%. The PCJ behavior is highly correlated with the main gallery pressure behavior, so it makes sense that it is behavior had a better fit to the models when using the main gallery pressure as input. This behavior is seen due to the mechanical configuration of the PCJ gallery in the engine. The results here shown are always comparing the estimated parameters using the estimation data with the validation data.

The level of accuracy achieved by the dynamic models was shown to have a NRMSE higher than 70% for all models presented here, even for the linear ones. The results obtained from the HW model can be considered the one that better describes the system by looking at its NRMSE. This representation was used to describe a digital twin of the real system. A significant advantage of using low-order regression models, such as the one proposed in this sutdy, is their simplicity of implementation, which makes them a suitable choice for embedded systems. For instance, the engine ECU can be a potential application of this model.

Conversely, it's noteworthy that numerous model configurations exhibited difficulty in capturing and generalizing the system's dynamics effectively. This behavior serves as a cautionary signal when considering the choice of a suitable model. Notably, nonlinear models with a higher degree of freedom demonstrated a propensity to overfit the training data. This overfitting phenomenon hindered their utility in the subsequent validation phase, rendering them

less versatile and reliable in real-world applications. It is possible to conclude the overfit of some models when checking the error values for the estimation phase and cross them against the results from the validation phase.

Future work includes exploring different types of model structures, such as testing grey-box strategies. An alternative approach would be to use various inputs and evaluate their correlation with the output signal to make more informed input selections. In this scenario, instead of using simple inputs, data from other actuators and sensors that could potentially impact the oil system, such as temperature readings at different points of the engine, could be utilized. Also, different combinations for the nonlinear models could be tested, since just a simple configuration was used for the NARX models and no different combinations for input non linearity and output non linearity were used for the HW models.

5.1 PUBLICATIONS

A paper based on this work called *System Identification Study to Model a Digital Twin for a Heavy-Duty Vehicle's Oil System* was presented at IEEE/IAS International Conference on Industry Applications (INDUSCON) 2023. Also, a journal paper is being prepared about the same work.

REFERENCES

AGARWAL, Deepak; KUMAR, Lokesh; AGARWAL, Avinash Kumar. Performance evaluation of a vegetable oil fuelled compression ignition engine. **Renewable energy**, Elsevier, v. 33, n. 6, p. 1147–1156, 2008.

AGRAWAL, Ajay K. 12 liquid fuel atomization and combustion. **Renewable Fuels: Sources, Conversion, and Utilization**, Cambridge University Press, p. 414, 2022.

AGUIRRE, Luis Antonio. **Introdução à identificação de sistemas–Técnicas lineares e não-lineares aplicadas a sistemas reais**. *[S.l.]*: Editora UFMG, 2004.

AGUIRRE, LUIS A; RODRIGUES, Giovani G; JÁCOME, Cristiano RF. Identificação de sistemas não lineares utilizando modelos narmax polinomiais–uma revisão e novos resultados. **SBA Controle e automação**, v. 9, n. 2, p. 90–106, 1998.

BILLINGS, Stephen A. **Nonlinear system identification: NARMAX methods in the time, frequency, and spatio-temporal domains**. *[S.l.]*: John Wiley & Sons, 2013.

BRACE, Christian J; HAWLEY, J Gary; COX, Allan; PEGG, IG; STARK, R. The effect of variable flow oil pumps on vehicle fuel economy. *In*: CHANDOS PUBLISHING. **Low-Carbon Vehicles 2009, May 20, 2009-May 21, 2009**. *[S.l.]*, 2009. p. 219–226.

BUSH, John Emmett; LONDON, Alexander Louis. Design data for" cocktail shaker" cooled pistons and valves. **SAE Transactions**, JSTOR, p. 446–459, 1966.

Engineers Edge. **Engine Lubrication - Engineers Edge**. 2023. Accessed on 8th September 2023. Available at: https://www.engineersedge.com/power_transmission/engine_lubrication.htm.

GLAESSGEN, Edward; STARGEL, David. The digital twin paradigm for future nasa and us air force vehicles. *In*: **53rd AIAA/ASME/ASCE/AHS/ASC structures, structural dynamics and materials conference 20th AIAA/ASME/AHS adaptive structures conference 14th AIAA**. *[S.l.: s.n.]*, 2012. p. 1818.

GRIEVES, Michael; VICKERS, John. Digital twin: Mitigating unpredictable, undesirable emergent behavior in complex systems. **Transdisciplinary perspectives on complex systems: New findings and approaches**, Springer, p. 85–113, 2017.

HOANG, Anh Tuan. Applicability of fuel injection techniques for modern diesel engines. *In*: AIP PUBLISHING. **AIP Conference Proceedings**. *[S.l.]*, 2020. v. 2207, n. 1.

HUANG, Tiexiong; HU, Guangdi; YAN, Yan; ZENG, Dongjian; MENG, Zhongwei. Combined feedforward and error-based active disturbance rejection control for diesel particulate filter thermal regeneration. **ISA transactions**, Elsevier, v. 134, p. 28–41, 2023.

JIANG, Kai; YAN, Fengjun; ZHANG, Hui. Data-driven control of automotive diesel engines and after-treatment systems: State of the art and future challenges. **Proceedings of the Institution of Mechanical Engineers, Part D: Journal of Automobile Engineering**, SAGE Publications Sage UK: London, England, p. 09544070221104893, 2022.

JONES, David; SNIDER, Chris; NASSEHI, Aydin; YON, Jason; HICKS, Ben. Characterising the digital twin: A systematic literature review. **CIRP journal of manufacturing science and technology**, Elsevier, v. 29, p. 36–52, 2020.

KLEIN, SA. An explanation for observed compression ratios in internal combustion engines. 1991.

LEE, Jay; LAPIRA, Edzel; YANG, Shanhu; KAO, Ann. Predictive manufacturing system-trends of next-generation production systems. **Ifac proceedings volumes**, Elsevier, v. 46, n. 7, p. 150–156, 2013.

LEITES, José M Martins; CAMARGO, Roberto C De. Articulated piston cooling optimization. **SAE Transactions**, JSTOR, p. 374–381, 1993.

LEONE, Thomas G; ANDERSON, James E; DAVIS, Richard S; IQBAL, Asim; REESE, Ronald A; SHELBY, Michael H; STUDZINSKI, William M. The effect of compression ratio, fuel octane rating, and ethanol content on spark-ignition engine efficiency. **Environmental science & technology**, ACS Publications, v. 49, n. 18, p. 10778–10789, 2015.

LIU, Zhongmin; ZHAI, Xin. Experimental study on the energy consumption of gasoline engine lubricating pumps in standardized driving cycles. **Mechanics Based Design of Structures and Machines**, Taylor & Francis, v. 51, n. 1, p. 450–463, 2023.

LJUNG, Lennart. System identification. *In*: **Signal analysis and prediction**. *[S.l.]*: Springer, 1998. p. 163–173.

LJUNG, Lennart. **Model validation and model error modeling**. *[S.l.]*: Linköping University Electronic Press, 1999.

LJUNG, Lennart *et al.* Theory for the user. **System identification**, Prentice-hall, Inc., 1987.

LOGANATHAN, S; GOVINDARAJAN, S; KUMAR, J Suresh; VIJAYAKUMAR, K; SRINIVASAN, K. **Design and development of vane type variable flow oil pump for automotive application**. *[S.l.]*, 2011.

LUBRICANTS, Wolf. **The Basics of Lubricants: How Does Engine Oil Work?** 2023. Accessed on 8th September 2023. Available at: https://www.wolflubes.com/en-us/news/the-basics-of-lubricants-how-does-engine-oil-work-5-9.

LUFF, David C; LAW, Theo; SHAYLER, Paul J; PEGG, Ian. The effect of piston cooling jets on diesel engine piston temperatures, emissions and fuel consumption. **SAE International Journal of Engines**, JSTOR, v. 5, n. 3, p. 1300–1311, 2012.

LUMSDEN, Grant; OUDENIJEWEME, Dave; FRASER, Neil; BLAXILL, Hugh. Development of a turbocharged direct injection downsizing demonstrator engine. **SAE International Journal of Engines**, JSTOR, v. 2, n. 1, p. 1420–1432, 2009.

MARATHE, Neelkanth V; WALKE, Nagesh H; JUTTU, Simhachalam; CHAUDHARI, Hitesh B; DEV, Subhankar; SAMANT, Mohak P. Introduction to thermal management techniques. **Handbook of Thermal Management of Engines**, Springer, p. 3–27, 2022.

MÜNCHHOF, Marco; ISERMANN, Rolf. **Identification of dynamical systems: An introduction with applications**. *[S.l.]*: Springer, 2011.

NAIK, Suramya; REDON, Fabien; REGNER, Gerhard; KOSZEWNIK, John. **Opposed-piston 2-stroke multi-cylinder engine dynamometer demonstration**. *[S.l.]*, 2015.

NEEDELMAN, William M; MADHAVAN, Puliyur V. Review of lubricant contamination and diesel engine wear. SAE Technical Paper, 1988.

NIKOLAKIS, Nikolaos; ALEXOPOULOS, Kosmas; XANTHAKIS, Evangelos; CHRYSSOLOURIS, George. The digital twin implementation for linking the virtual representation of human-based production tasks to their physical counterpart in the factory-floor. **International Journal of Computer Integrated Manufacturing**, Taylor & Francis, v. 32, n. 1, p. 1–12, 2019.

PANETTA, Kasey. **Gartner Top 10 Strategic Technology Trends for 2019**. 2018. Accessed on October 15, 2018. Available at: https://www.gartner.com/smarterwithgartner/gartner-top-10-strategic-technology-trends-for-2019/.

REIF, Konrad. **Dieselmotor-management im Überblick**. *[S.l.]*: Springer, 2010.

SMITS, Volker; SCHÜSSLER, Max; KAMPMANN, Geritt; ILLG, Christopher; DECKER, Tim; NELLES, Oliver. Excitation signal design and modeling benchmark of nox emissions of a diesel engine. *In*: IEEE. **2022 IEEE Conference on Control Technology and Applications (CCTA)**. *[S.l.]*, 2022. p. 907–912.

TAO, Gang; TIAN, Ming. Discrete-time adaptive control of systems with multisegment piecewise-linear nonlinearities. **IEEE transactions on automatic control**, IEEE, v. 43, n. 5, p. 719–723, 1998.

THOMAS, K Mark. The release of nitrogen oxides during char combustion. **Fuel**, Elsevier, v. 76, n. 6, p. 457–473, 1997.

TING, Yew Siang. **A study of upward oil jet impingement on flat and concave heated surfaces and the application to IC engine piston cooling**. 2007. Phd Thesis (PhD Thesis) — Loughborough University, 2007.

TRAUER, Jakob; SCHWEIGERT-RECKSIEK, Sebastian; ENGEL, Carsten; SPREITZER, Karsten; ZIMMERMANN, Markus. What is a digital twin?–definitions and insights from an industrial case study in technical product development. *In*: CAMBRIDGE UNIVERSITY PRESS. **Proceedings of the design society: DESIGN conference**. *[S.l.]*, 2020. v. 1, p. 757–766.

WANG, De Ming; DING, Hui; JIANG, Yu; XIANG, Xin. **Numerical modeling of vane oil pump with variable displacement**. *[S.l.]*, 2012.

WANG, Xingzhi; WANG, Yuchen; TAO, Fei; LIU, Ang. New paradigm of data-driven smart customisation through digital twin. **Journal of manufacturing systems**, Elsevier, v. 58, p. 270–280, 2021.

XIN, Qianfan. **Diesel engine system design**. *[S.l.]*: Elsevier, 2011.

ZHANG, Tantan. An estimation method of the fuel mass injected in large injections in common-rail diesel engines based on system identification using artificial neural network. **Fuel**, Elsevier, v. 310, p. 122404, 2022.

ZHANG, Wei; WANG, Bin; ZHANG, Yanhuan; PENG, Lele; LIU, Mohan; LV, Yancheng. Research on modelling and simulation of a new variable displacement oil pump. **The Journal of Engineering**, v. 2019, 01 2019.

ANNEX

ANNEX A – DIREITOS AUTORAIS - LEI N.º 9.610, DE 19 DE FEVEREIRO DE 1998: DISPOSIÇÕES PRELIMINARES

Presidência da República
Casa Civil
Subchefia para Assuntos Jurídicos

LEI Nº 9.610, DE 19 DE FEVEREIRO DE 1998.

Mensagem de veto

Vide Lei nº 12.853, de 2013 (Vigência)

Altera, atualiza e consolida a legislação sobre direitos autorais e dá outras providências.

O PRESIDENTE DA REPÚBLICA Faço saber que o Congresso Nacional decreta e eu sanciono a seguinte Lei:

Título I

Disposições Preliminares

Art. 1º Esta Lei regula os direitos autorais, entendendo-se sob esta denominação os direitos de autor e os que lhes são conexos.

Art. 2º Os estrangeiros domiciliados no exterior gozarão da proteção assegurada nos acordos, convenções e tratados em vigor no Brasil.

Parágrafo único. Aplica-se o disposto nesta Lei aos nacionais ou pessoas domiciliadas em país que assegure aos brasileiros ou pessoas domiciliadas no Brasil a reciprocidade na proteção aos direitos autorais ou equivalentes.

Art. 3º Os direitos autorais reputam-se, para os efeitos legais, bens móveis.

Art. 4º Interpretam-se restritivamente os negócios jurídicos sobre os direitos autorais.

Art. 5º Para os efeitos desta Lei, considera-se:

I - publicação - o oferecimento de obra literária, artística ou científica ao conhecimento do público, com o consentimento do autor, ou de qualquer outro titular de direito de autor, por qualquer forma ou processo;

II - transmissão ou emissão - a difusão de sons ou de sons e imagens, por meio de ondas radioelétricas; sinais de satélite; fio, cabo ou outro condutor; meios óticos ou qualquer outro processo eletromagnético;

III - retransmissão - a emissão simultânea da transmissão de uma empresa por outra;

IV - distribuição - a colocação à disposição do público do original ou cópia de obras literárias, artísticas ou científicas, interpretações ou execuções fixadas e fonogramas, mediante a venda, locação ou qualquer outra forma de transferência de propriedade ou posse;

V - comunicação ao público - ato mediante o qual a obra é colocada ao alcance do público, por qualquer meio ou procedimento e que não consista na distribuição de exemplares;

VI - reprodução - a cópia de um ou vários exemplares de uma obra literária, artística ou científica ou de um fonograma, de qualquer forma tangível, incluindo qualquer armazenamento permanente ou temporário por meios eletrônicos ou qualquer outro meio de fixação que venha a ser desenvolvido;

VII - contrafação - a reprodução não autorizada;

VIII - obra:

a) em co-autoria - quando é criada em comum, por dois ou mais autores;

b) anônima - quando não se indica o nome do autor, por sua vontade ou por ser desconhecido;

c) pseudônima - quando o autor se oculta sob nome suposto;

d) inédita - a que não haja sido objeto de publicação;

e) póstuma - a que se publique após a morte do autor;

f) originária - a criação primígena;

g) derivada - a que, constituindo criação intelectual nova, resulta da transformação de obra originária;

h) coletiva - a criada por iniciativa, organização e responsabilidade de uma pessoa física ou jurídica, que a publica sob seu nome ou marca e que é constituída pela participação de diferentes autores, cujas contribuições se fundem numa criação autônoma;

i) audiovisual - a que resulta da fixação de imagens com ou sem som, que tenha a finalidade de criar, por meio de sua reprodução, a impressão de movimento, independentemente dos processos de sua captação, do suporte usado inicial ou posteriormente para fixá-lo, bem como dos meios utilizados para sua veiculação;

IX - fonograma - toda fixação de sons de uma execução ou interpretação ou de outros sons, ou de uma representação de sons que não seja uma fixação incluída em uma obra audiovisual;

X - editor - a pessoa física ou jurídica à qual se atribui o direito exclusivo de reprodução da obra e o dever de divulgá-la, nos limites previstos no contrato de edição;

XI - produtor - a pessoa física ou jurídica que toma a iniciativa e tem a responsabilidade econômica da primeira fixação do fonograma ou da obra audiovisual, qualquer que seja a natureza do suporte utilizado*;*

XII - radiodifusão - a transmissão sem fio, inclusive por satélites, de sons ou imagens e sons ou das representações desses, para recepção ao público e a transmissão de sinais codificados, quando os meios de decodificação sejam oferecidos ao público pelo organismo de radiodifusão ou com seu consentimento;

XIII - artistas intérpretes ou executantes - todos os atores, cantores, músicos, bailarinos ou outras pessoas que representem um papel, cantem, recitem, declamem, interpretem ou executem em qualquer forma obras literárias ou artísticas ou expressões do folclore.

XIV - titular originário - o autor de obra intelectual, o intérprete, o executante, o produtor fonográfico e as empresas de radiodifusão. (Incluído pela Lei nº 12.853, de 2013)

Art. 6º Não serão de domínio da União, dos Estados, do Distrito Federal ou dos Municípios as obras por eles simplesmente subvencionadas.